Estimating time in quantum chaotic systems and black holes

Haifeng Tang [1†], Shreya Vardhan[1⋆], and Jinzhao Wang[1‡]

1 Stanford Institute for Theoretical Physics, Stanford University, Stanford, CA 94305, USA

† hftang@stanford.edu ,   ⋆ shreyavar08@gmail.com ,   † jinzhao@stanford.edu

Abstract

We characterize new universal features of the dynamics of chaotic quantum many-body systems, by considering a hypothetical task of "time estimation." Most macroscopic observables in a chaotic system equilibrate to nearly constant late-time values. Intuitively, it should become increasingly difficult to estimate the precise value of time by making measurements on the state. We use a quantity called the Fisher information from quantum metrology to quantify the minimum uncertainty in estimating time. Due to unitarity, the uncertainty in the time estimate does not grow with time if we have access to optimal measurements on the full system. Restricting the measurements to act on a small subsystem or to have low computational complexity leads to results expected from equilibration, where the time uncertainty becomes large at late times. With optimal measurements on a subsystem larger than half of the system, we regain the ability to estimate the time very precisely, even at late times.

Hawking's calculation for the reduced density matrix of the black hole radiation in semiclassical gravity contradicts our general predictions for unitary quantum chaotic systems. Hawking's state always has a large uncertainty for attempts to estimate the time using the radiation, whereas our general results imply that the uncertainty should become small after the Page time. This gives a new version of the black hole information loss paradox in terms of the time estimation task. By restricting to simple measurements on the radiation, the time uncertainty becomes large. This indicates from a new perspective that the observations of computationally bounded agents are consistent with the semiclassical effective description of gravity.

Contents

29

30

1   Introduction

32   At late times in chaotic quantum many-body systems, most simple macroscopic observables
33   relax to steady-state values, which are constant with time up to small fluctuations. Intuitively,
34   from the perspective of such observables, the evolution of the state $|\psi(t)\rangle = e^{-iHt}|\psi_0\rangle$ by
35   the chaotic Hamiltonian H from any initial state $|\psi_0\rangle$ slows down with time. This intuition is
36   captured by the fact that the late-time state $|\psi(t)\rangle$ macroscopically resembles an equilibrium
37   density matrix $\rho^{(eq)}$, which commutes with the Hamiltonian and does not evolve at all. In this
38   paper, we will explore the extent to which the state $|\psi(t)\rangle$ evolves with t using a hypothetical
39   task of "time estimation." We imagine that we are given an $\mathcal{O}(1)$ number of copies of $|\psi(t)\rangle$,
40   but do not know the precise value of t and want to estimate it using measurements on the
41   state. How effectively can we perform this task?

42   The setup of this thought experiment is inspired by the general task of parameter estima-
43   tion in quantum metrology [1, 2]. We use a quantity called the Fisher information [3–5] to
44   quantify the minimum uncertainty in the time estimate. Studying the behaviour of the Fisher
45   information for time estimation will allow us to identify certain universal features of thermal-
46   ization beyond those captured by standard observables including correlation functions and
47   entanglement entropy. This approach contributes a new perspective to recent discussions on
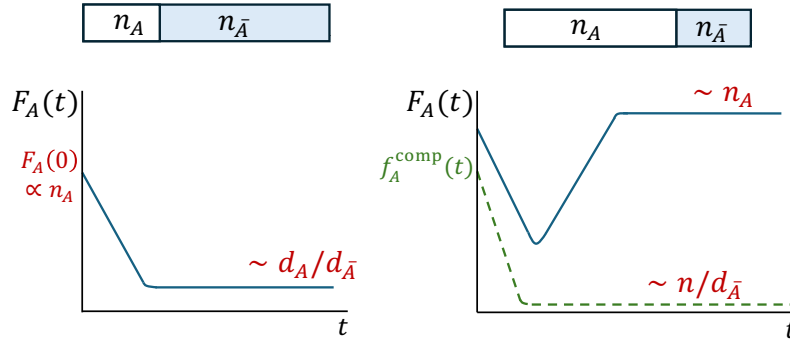
Figure 1: We consider the evolution of the subsystem Fisher information associated with time estimation in a chaotic quantum many-body system. We divide the system into two parts A and $\bar{A}$, and n_A, d_A respectively denote the number of degrees of freedom and Hilbert space dimension of A. For $n_A < n_{\bar{A}}$ (left), the subsystem quantum Fisher information $F_A(t)$ decays monotonically from an extensive value to an exponentially small value at late times, consistent with the expectation from thermalization. For $n_A > n_{\bar{A}}$ (right, blue curve), $F_A(t)$ shows a surprising non-monotonic evolution and saturates to an extensive value. On restricting to simple measurements, the associated classical Fisher information $f_A^{\text{comp}}(t)$ decays monotonically and becomes small even for $n_A > n/2$ (right, green dashed curve).

characterizing various fine-grained aspects of the structure of thermalizing quantum states, such as complexity growth [6], deep thermalization [7], subsystem entropy fluctuations [8], and pseudoentanglement [9, 10]. Further, by treating black holes as examples of chaotic systems, this quantity will allow us to identify a new version of Hawking's information loss paradox, and to make new predictions based on unitarity for the black hole evaporation process.

The Fisher information we will study can be seen as an intrinsic velocity associated with changes in the state with time. The minimum uncertainty $(\delta t)^2$ of an attempted time estimate is inversely proportional to the Fisher information. Intuition from thermalization suggests that the Fisher information should decay and go to zero at late times, corresponding to a large uncertainty of time estimation. However, there is a competing intuition from unitarity that $|\psi(t)\rangle$ cannot stop evolving with time at a fundamental microscopic level. We will see that the latter intuition is captured by the fact that an optimal version of the Fisher information, known as the quantum Fisher information (QFI), is a constant with time if we have access to the full system. This constant value is proportional to the energy variance of the state. Hence, the full microscopic state $|\psi(t)\rangle$ evolves just as fast at any later time as it does initially.

With optimal measurements on the full system, we therefore always retain the ability to estimate time accurately if we could do so at early times. We consider two natural kinds of sub-optimal measurements. The uncertainty in time on considering optimal measurements on a subsystem is quantified by the *subsystem quantum Fisher information* $F_A(t)$. On the other hand, by restricting the *computational complexity* of measurements, either on the full system or on a subsystem, we naturally arrive at another coarse-grained Fisher information called the *classical Fisher information* in the computational basis, $f_A^{\text{comp}}(t)$. $F_A(t)$ for a subsystem smaller than half of the system, and $f_A^{\text{comp}}(t)$ even for more than half of the system, will both turn out to reproduce expectations from thermalization. We will define these quantities and introduce the task of time estimation more explicitly in Sec. 2.

We summarize our main results in the schematic plots in Fig. 1. These results apply to pure initial states with extensive energy variance, which also have extensive initial values of F_A and f_A^{comp}. Based on results in spin chains, random pure states, and other toy models,

76 we expect that these behaviours should be universal for unitary chaotic quantum many-body
77 systems with local interactions.

78 Let $n_A, n_{\bar{A}}$ denote the number of degrees of freedom in a subsystem A and its complement
79 $\bar{A}$. The full system size is n. We find two striking differences between the subsystem quantum
80 Fisher information $F_A(t)$ between the cases $n_A < n_{\bar{A}}$ and $n_A > n_{\bar{A}}$ as shown in Fig. 1, which are
81 consequences of the interplay between thermalization and unitarity:

1. The saturation value of $F_A(t)$ is exponentially suppressed in n for $n_A < n_{\bar{A}}$, and propor-
   tional to n for $n_A > n_{\bar{A}}$. This transition can be understood from Haar-random pure states.
   Like previous transitions at $n_A = n/2$ found by Page [11] and Hayden and Preskill [12],
   this transition indicates a qualitative difference between $\mathrm{Tr}_{\bar{A}}[|\psi(t)\rangle\langle\psi(t)|]$ and the equi-
   librium density matrix $\mathrm{Tr}_{\bar{A}}[\rho^{(\mathrm{eq})}]$ when we consider a subsystem larger than half of the
   system. The new transition indicates a difference in the *speed of evolution* of the two
   states, rather than in their *information content* which is captured by entanglement en-
   tropy.

2. For $n_A < n_{\bar{A}}$, $F_A(t)$ shows a monotonic decay with time, consistent with the physical
   expectation that the time-evolution is increasingly slowing down. For $n_A > n_{\bar{A}}$, $F_A(t)$
   shows a non-monotonic time-evolution. [1] We will understand the increasing behaviour
   at intermediate times, which is counterintuitive from the perspective of thermalization,
   as follows. $\rho_A(t)$ is not full-rank for $n_A > n_{\bar{A}}$, and its support rotates within the full
   Hilbert space of A. As the state gains access to more and more of the Hilbert space, its
   speed of rotation increases, until it saturates to a universal late-time value which gives
   the dominant contribution to $F_A(t)$. See Fig. 2.

   Note that more conventional probes of thermalization such as entanglement entropy
   are insensitive to any properties of the eigenstates of the reduced density matrices and
   cannot capture this physical phenomenon.

101 We also study the behaviour of $F_A(t)$ in a free-fermion integrable system and find a remark-
102 ably different behaviour, indicating that this quantity is a sharp probe of the transition from
103 integrability to chaos.

104 In a chaotic system, even for $n_A > n_{\bar{A}}$, we find that the Fisher information f_A^{comp} associated
105 with simple measurements shows a monotonic decay and saturates to an exponentially small
106 value in n. This is true as long as $n_A < n - \mathcal{O}(\log n)$, after which point even f_A^{comp} is no longer
107 small.

108 Let us now turn to the implications of these results for black holes, by treating them as
109 examples of highly chaotic quantum many-body systems. The process of formation of a black
110 hole from a star corresponds to the approach to equilibrium in general chaotic systems. Hawk-
111 ing [13,14] found that black holes subsequently emit thermal radiation and evaporate. How-
112 ever, Hawking's calculation of the state of the black hole radiation in semiclassical gravity leads
113 to a contradiction with the above general predictions for unitary evolutions. This can be seen
114 as a new version of the black hole information paradox, now relating to the time-evolution
115 properties of the state rather than its entropy.

116 According to Hawking, the density matrix of the radiation in the evaporation process is
117 given by a thermal density matrix. While the black hole mass M gradually decreases during
118 the evaporation process, on shorter time scales $|\delta t| \ll \delta t_{\mathrm{evap}} \equiv G_N M$ the density matrix
119 of the radiation in Hawking's state is a stationary equilibrium state $\rho^{(\mathrm{eq})}$ corresponding to
120 temperature $T_H = 1/(8\pi G_N M)$. If we treat the times scale $\delta t_{\mathrm{evap}} = G_N M$ as infinite, then

---

[1]The decay is monotonic up to small fluctuations which go away on averaging over initial states or small time intervals.
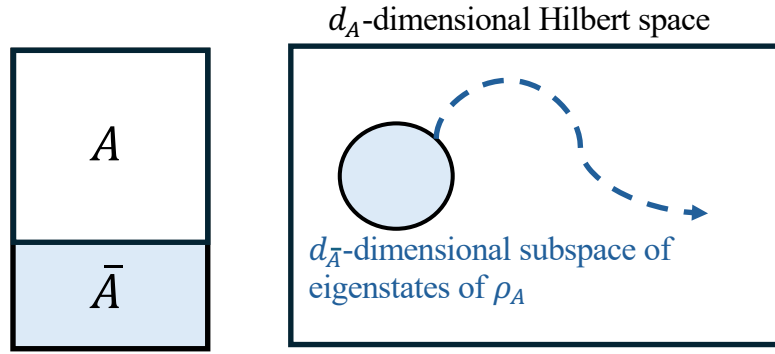
Figure 2: For a pure state $|\psi(t)\rangle$ in a chaotic system, for a subsystem A larger than half of the system, the QFI of the reduced density matrix $\rho_A(t)$ has a large universal late-time value. In this case, $\rho_A(t)$ is not full-rank. The late-time value of the QFI captures the speed of rotation of the support of $\rho_A(t)$ within the full Hilbert space of A.

$\rho^{(\mathrm{eq})}$ does not evolve, and the value of the subsystem QFI of the radiation according to the naive calculation in semiclassical gravity is therefore zero.

Based on similar reasoning to earlier works of Page [11, 15] and Hayden and Preskill [12], we expect that the universal behaviours that we find for the quantum Fisher information in chaotic quantum many-body systems should also apply to black holes in their fundamental description. This implies that in the fundamental description, Hawking's result of zero subsystem QFI of the radiation cannot be true after the Page time, when the effective Hilbert space dimension of the radiation becomes larger than that of the black hole. Instead, we predict that the subsystem QFI of the radiation should become $\mathcal{O}(1/G_N)$ after the Page time in the fundamental description of the black hole. This implies that the time can be estimated to a precision $|\delta t| \sim \sqrt{G_N}$ using optimal measurements on the radiation after the Page time. In particular, this uncertainty is much smaller than the uncertainty $\sim \delta t_{\mathrm{evap}} = G_N M$ with which one could naively estimate time by measuring changes in the energy or temperature of the radiation, as long as the black hole mass is larger than the Planck mass ($M \gg 1/\sqrt{G_N}$). It would be interesting to see whether and how our predictions for the subsystem QFI can be checked by including corrections to semiclassical gravity, such as those that were recently used to obtain the Page curve in [16–19].

The optimal measurements on the radiation that lead to a small uncertainty of the time estimate after the Page time are likely to be highly complex. There is a growing body of evidence in the literature that observations made by computationally bounded observers with access to the radiation are consistent with Hawking's semiclassical calculation for the reduced density matrix of the radiation [20–25]. Our results for the computational basis classical Fisher information f_A^{comp} provide yet another perspective that confirms these ideas. We predict that the value of this quantity is $\mathcal{O}(e^{-1/G_N})$ at all but very late times in the evaporation process. Hence, it is effectively indistinguishable from the result of zero Fisher information from Hawking's state.

The plan of the paper is as follows. In Sec. 2, we explain the setup of the time estimation task, introduce the relevant quantities, and discuss general constraints on them from unitary Hamiltonian evolution. In Sec. 3, we discuss results for the quantum Fisher information associated with subsystems using a variety of models for chaotic systems, as well as an example of an integrable system. In Sec. 4, we discuss the classical Fisher information for simple measurements in the computational basis. In Sec. 5, we carry out an explicit numerical simulation where we estimate the value of time by making measurements on the state, using a method

called the maximum likelihood estimate. In addition to being a fun experiment, this clarifies a conceptual question about whether it is possible to come up with a global (as opposed to merely local) estimate of time when the Fisher information is large. In Sec. 6, we phrase our question about time estimation in the language of quantum error-correction in order to make an explicit comparison between the task we consider here and the Hayden-Preskill protocol. Most technical details are presented in the Appendices.

We expect the results to be of equal interest from the perspective of quantum many-body physics and quantum gravity. The sections most relevant in the context of black hole physics are Sec. 3.3 on results in random pure states, Sec. 3.4 about the implications of these results for black holes, and the discussions in Sec. 4 and Sec. 5 on the complexity of distinguishing the time-evolved state from the thermal state (or equivalently, distinguishing the fundamental description of the black hole from Hawking's description).

Relation to previous work: The QFI has previously been applied to quantum many-body systems in the context of dynamical susceptibilities and multipartite entanglement [26–28]. In these setups, the parameter to be estimated is associated with deformations of the state by operators other than the Hamiltonian. The physical interpretation of the QFI in such cases is different from the one in this paper. The QFI associated with time estimation was previously considered in [29], with a different goal of characterizing time-energy uncertainty relations. In the context of classical stochastic dynamics, the Fisher information associated with time estimation was studied in [30]. The models in [30] can be seen as coarse-grained, classical descriptions of thermalization, which we will contrast with microscopic quantum-mechanical descriptions. In [31], a particular case of our time estimation task, using simple measurements on the full system, was studied using a different but related quantity and the authors arrived at similar conclusions.

2   Setup and constraints from unitarity

In the setup of our thought experiment, we will consider two kinds of one-parameter families of states, labelled by the parameter t: either the time-evolved state on the full system, $\sigma(t) = e^{-iHt}\sigma_0 e^{iHt}$ for some initial state σ_0, or its reduced density matrix on some subsystem, $\sigma_A(t) = \mathrm{Tr}_{\bar{A}}[e^{-iHt}\sigma_0 e^{iHt}]$, where $\bar{A}$ is the complement of A. Let us denote these two cases by the common notation $\rho(t)$. Suppose we are experimentalists who are given N copies of $\rho(t_0)$, at a particular value t_0 of t. We know the initial state σ_0 and H, but do not know t_0, and want to estimate its value by making measurements on our N copies.

Consider some choice of complete projective measurement, with measurement outcomes labelled by $|\xi\rangle$. From N independent measurements on $\rho(t_0)$, we obtain measurement outcomes $\xi_1, ..., \xi_N$. Suppose we come up with an estimate $T_{\text{est}}(\xi_1, ..., \xi_N)$ for t_0 based on these measurement outcomes. Our key question is the following: how well can the best possible function T_{est} do at estimating t_0? If no estimator is able to do a good job, this indicates that $\rho(t)$ is not changing much with t, at least with respect to the measurement basis $\{|\xi\rangle\}$.

We can quantify the accuracy of the estimator T_{est} using the following measure:

$$
\begin{aligned}
(\delta T_{\text{est}})^2 &\equiv \overline{(T_{\text{est}}(\xi_1, ..., \xi_N) - t_0)^2} \\
&= \sum_{\xi_1, ..., \xi_N} p_{\xi_1}(t_0) ... p_{\xi_N}(t_0) \, (T_{\text{est}}(\xi_1, ..., \xi_N) - t_0)^2 \, , \\
& \quad\quad p_\xi(t) \equiv \langle \xi | \rho(t) | \xi \rangle \, ,
\end{aligned}
\tag{1}
$$

where the sum of each ξ_i is over all possible values of ξ_i. Based on the general theory of statistical inference of a parameter in a probability distribution using samples from the distribution,

195 $(\delta T_{\text{est}})^2$ has a known lower bound over all possible choices of T_{est}. This lower bound can be
196 expressed in terms of intrinsic properties of the family of probability distributions $p_\xi(t)$:

$$(\delta T_{\text{est}})^2 \geq \frac{1}{NF(t_0)}, \quad f(t_0) \equiv \sum_\xi \frac{1}{p_\xi(t_0)} \left(\frac{\partial p_\xi(t)}{\partial t} \bigg|_{t_0} \right)^2, \tag{2}$$

197 where $f(t_0)$ is known as the Fisher information for the probability distribution $p_\xi(t)$ at $t = t_0$.
198 The above inequality is known as the Cramer-Rao bound, and can be saturated by a known
199 form of T_{est} for large N, known as the maximum likelihood estimate (MLE) [32, 33]. We will
200 discuss further details of the MLE and its explicit implementation in Sec. 5.

201 For a quantum state $\rho(t)$, it is natural to consider the maximum value of the Fisher in-
202 formation over all possible choices of the measurement basis $\{|\xi\rangle\}$. This maximum value is
203 known as the quantum Fisher information (QFI) [4], and has the following explicit formula:

$$F(t) \equiv \text{Tr}\left[\frac{\partial \rho}{\partial t} \mathcal{R}_\rho^{-1} \left(\frac{\partial \rho}{\partial t} \right) \right], \tag{3}$$

$$\mathcal{R}_\rho^{-1}(\cdot) \equiv \sum_{\substack{i,j \text{ s.t.} \\ p_i + p_j \neq 0}} \frac{2}{p_i + p_j} |\psi_i\rangle \langle \psi_i| (\cdot) |\psi_j\rangle \langle \psi_j|. \tag{4}$$

204 Here p_i and $|\psi_i\rangle$ are respectively the eigenvalues and eigenstates of $\rho(t)$. [2] As discussed
205 in [4], the QFI equivalent to a certain distance measure known as the Bures distance between
206 the states at t and $t + dt$:

$$F(t) = 4 \lim_{dt \to 0} \frac{d_{\text{Bures}}(\rho(t), \rho(t + dt))^2}{dt^2},$$

$$d_{\text{Bures}}(\rho, \sigma) \equiv \sqrt{2} \left(1 - \text{Tr}\left[\sqrt{\sqrt{\rho}\sigma\sqrt{\rho}} \right] \right)^{\frac{1}{2}}. \tag{5}$$

207 It is therefore natural to view the QFI for time estimation as an intrinsic velocity associated
208 with changes in the state.

209 Note that since the optimal projective measurement basis is the eigenbasis of $\mathcal{R}_\rho^{-1}(\partial \rho / \partial t|_{t_0})$,
210 it depends on t_0 itself. Hence, the quantum Fisher information is the uncertainty $(\delta T_{\text{est}})^2$ as-
211 sociated with attempts to locally estimate values of time $t_0' = t_0 + \Delta t$ *close to* t_0, and assuming
212 knowledge of t_0.

213 So far, our discussion was completely general, and would apply to any one-parameter
214 family $\rho(X)$ labelled by some continuous variable X. Let us now consider turn to the value of
215 QFI on taking $\rho(t) = e^{-iHt} \sigma_0 e^{iHt}$, i.e., the time-evolved state on the full system. In this case,
216 we find that the QFI is constant with respect to t. For an initial pure state $|\psi_0\rangle$, the QFI at all
217 times is proportional to the energy variance:

$$F(t) = F(0) = 4 \left(\langle H^2 \rangle_{\psi_0} - \langle H \rangle_{\psi_0}^2 \right) \tag{6}$$

218 where $\langle \cdots \rangle_\psi$ indicates expectation values in $|\psi\rangle$. In particular, this implies that the QFI is
219 zero at all times for an energy eigenstate, consistent with the fact that an eigenstate does
220 not show any non-trivial time-evolution. On the other hand, a product state in a local lattice
221 system has energy variance of $\mathcal{O}(n)$, where n is the number of sites, [3] indicating that the

---

[2]The superoperator $\mathcal{R}_\rho^{-1}(\cdot)$ is the inverse of $\mathcal{R}_\rho(\cdot) \equiv \{\rho, \cdot\}$. $\mathcal{R}_\rho^{-1}(\partial_t \rho)$ is known as the symmetric logarithmic derivative of ρ.

[3]Let the Hamiltonian be a sum of local terms $H = \sum_i h_i$. The energy variance is $\text{Var}(H) = \sum_{ij} \langle h_i h_j \rangle_{\psi_0} - \langle h_i \rangle_{\psi_0} \langle h_j \rangle_{\psi_0}$, and for a product state $\langle h_i h_j \rangle_{\psi_0}$ factorizes when h_i, h_j have no common support. Hence, the sum is restricted to $i \approx j$ and consists of $\mathcal{O}(n)$ terms each of $\mathcal{O}(1)$ magnitude.

optimal uncertainty $(\delta T_{\text{est}})^2$ is very small in the thermodynamic limit. This result is true for any Hamiltonian. It can be seen as a purely kinematical result of unitarity which is insensitive to thermalization, similar to the fact that the von Neumann entropy of the state on the full system is invariant under unitary evolution.

One can check that for a pure state, the optimal measurement basis [4], given by the eigenbasis of $\mathcal{R}_\rho^{-1}([H, |\psi(t)\rangle\langle\psi(t)|])$, consists of the states

$$\frac{1}{\sqrt{2}}(|\psi(t)\rangle \pm i\,|\xi(t)\rangle)\,,\ |\xi(t)\rangle \equiv \frac{(H - \langle H\rangle_\psi)}{\sqrt{\langle H^2\rangle_\psi - \langle H\rangle_\psi^2}}\,|\psi(t)\rangle\,, \tag{7}$$

and any set of $2^n - 2$ states that form an orthonormal basis together with these two states. The optimal measurements on the full system, for which the time uncertainty is determined by the constant QFI (6), are therefore as complex as the state $|\psi(t)\rangle$ itself and become increasingly complex at late times.

As discussed in the introduction, from the intuition about thermalization that a state evolved by a chaotic Hamiltonian relaxes to a steady state, we may expect the Fisher information to decay monotonically and go to zero at late times. Indeed, [30] previously studied the evolution of the classical Fisher information associated with time-evolution for a probability distribution evolved by the Fokker-Planck equation, which describes relaxation dynamics, and found results consistent with this intuition. We have seen above that the QFI on the full system shows a very different behaviour due to unitarity. In order to see results that match our expectations from thermalization, it is therefore necessary to put certain restrictions on the measurements we can perform to try to estimate the time.

One natural restriction is that the measurements can only act on some subsystem A of the full system, which corresponds to taking $\rho(t) = \sigma_A(t) = \text{Tr}_{\bar{A}}[e^{-iHt}\sigma_0 e^{iHt}]$ in (3), and yields the quantity

$$F_A(t) = \sum_{\substack{i,j \text{ s.t.} \\ p_i + p_j \neq 0}} \frac{2}{p_i + p_j} |\,\langle i|\text{Tr}_{\bar{A}}\big[H, e^{-iHt}\sigma_0 e^{iHt}\big]|j\rangle\,|^2 \tag{8}$$

where $p_i, |i\rangle$ are eigenvalues and eigenstates of $\sigma_A(t)$ (we do not show the time-dependence of these eigenvalues and eigenstates explicitly for conciseness). We will refer to (8) as the *subsystem QFI*. When the initial state is pure, recall that we can write a Schmidt decomposition of the time-evolved state as follows:

$$|\psi(t)\rangle = \sum_{i=1}^{\min(d_A, d_{\bar{A}})} \sqrt{p_i}\,|i\rangle_A\,|\tilde{i}\rangle_{\bar{A}} \tag{9}$$

where $p_i, |i\rangle_A, |\tilde{i}\rangle_{\bar{A}}$ are time-dependent but we do not show the time-dependence explicitly. We give an expression for $F_A(t)$ in Appendix A that depends on $H, p_i, |i\rangle_A, |\tilde{i}\rangle_{\bar{A}}$. This expression will be useful for later calculations. It is also conceptually interesting to note that $F_A(t)$ thus depends not only on the eigenvalues of $\rho_A(t)$ but also on the global structure of the state, including the eigenstates of ρ_A as well as $\rho_{\bar{A}}$ and their relation to the Hamiltonian H. This is in contrast to most information-theoretic quantities that are often studied for the time-evolved state such as the von Neumann and Renyi entropies, which depend only on the eigenvalues p_i. [4] In Section 3, we will discuss the behaviour of the subsystem QFI in quantum many-body systems.

Another natural restriction we can put on the measurements that we used to estimate the time is to require them to be simple in the sense of computational complexity. We can

---

[4] Another set of recently introduced quantities that probe the global structure of the state $|\psi(t)\rangle$ in a different way are "state k-design" frame potentials introduced in the context of deep thermalization [7, 31, 34–37].

quantify the uncertainty of the time estimate using a general measurement basis $\{|\xi\rangle\}$ with the classical Fisher information (CFI) for that basis $f(t)$, defined in (2). The simplest choice is to take $\{|\xi\rangle\}$ to be the computational basis, which we will call $f^{\mathrm{comp}}(t)$. We will discuss this case in Section 4.

3 Quantum fisher information for subsystems

In this section, we will study the behavior of the subsystem QFI $F_A(t)$ defined in (8). We will be interested mostly in chaotic systems with local interactions. We will consider initial states for which the constraints from energy conservation are not very important at late times, such that $|\psi(t)\rangle = e^{-iHt}|\psi_0\rangle$ macroscopically resembles the infinite temperature thermal density matrix $\mathbf{1}/d$ in terms of correlation functions and entanglement entropies of small subsystems. We expect that more general initial states with extensive energy variance should show similar behaviours, and will propose generalizations of some of our results to these cases.

In Fig. 1, we highlighted various qualitative features of the evolution of $F_A(t)$. Recall that we refer to the number of degrees of freedom and Hilbert space dimension of subsystem A as n_A, d_A respectively. Let us further summarize some additional features, which we expect should be robust in local chaotic systems:

1. $F_A(t)$ for $n_A < n_{\bar{A}}$ has an exponentially decaying regime at intermediate to late times before saturation:

$$F_A(t) \sim e^{-\alpha_{n_A} t} \, , \tag{10}$$

   where α_{n_A} has an inverse power law dependence on n_A, $\alpha_{n_A} \sim 1/n_A^\eta$ for some $\eta \geq 1$.

2. For $n_A > n_{\bar{A}}$, the time scale t^* corresponding to the minimum of $F_A(t)$ in Fig. 1 obeys $t^* \sim n_{\bar{A}}$.

3. The saturation value of $F_A(t)$ is

$$F_A \propto \begin{cases} n_A d_A / d_{\bar{A}} & n_A < n_{\bar{A}} \\ n_A & n_A > n_{\bar{A}} \end{cases} \tag{11}$$

   where the proportionality constant has units of energy density squared.

We make use of the following models to identify these features and provide evidence for their universality:

1. The mixed-field Ising model at generic values of the coupling exhibits each of the features summarized in the figure and the above points 1-3. This spin chain model is often used in the literature to probe universal characteristics of local chaotic dynamics. We present the numerical results from this model in Sec. 3.1. We also consider an integrable version of the spin chain, where we find a strikingly different behaviour of $F_A(t)$ for $n_A < n_{\bar{A}}$.

2. The exponential regime (10) for $n_A < n_{\bar{A}}$ is relatively short-lived in the spin chain model before it saturates for the system sizes we can access numerically. To better understand this decay, we model the smaller subsystem A as an open quantum system with boundary dissipation. This serves as a good qualitative model for the time-dependence, which allows us to better understand the form and physical origin of the n_A-dependent decay rate in (10). By construction, this model cannot give the saturation values (11) observed in unitary systems.
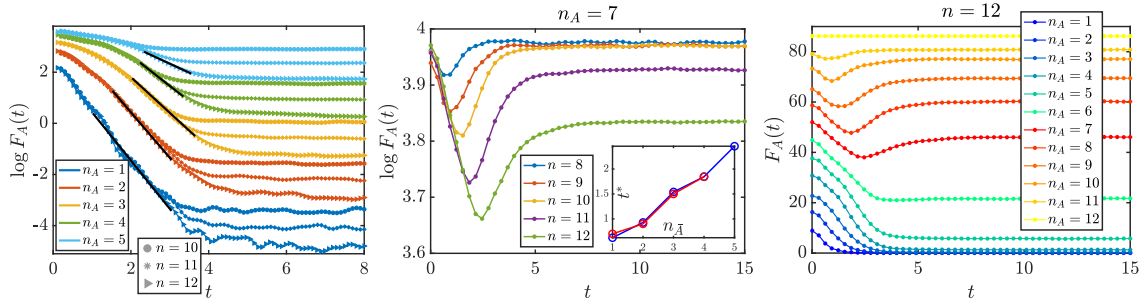
Figure 3: We plot the dynamics of $F_A(t)$ in the chaotic spin chain model (14) with various n and n_A. We evolve the system from random product initial states and average $F_A(t)$ over 200 samples of initial states for $n \leq 11$ and 84 samples for $n = 12$. **Left:** We focus on cases with $n_A \leq n/2$. The solid black lines show the fitting to exponential decay. The rate of exponential decay decreases with n_A and is independent of $n_{\bar{A}}$. (The decay rates α_{n_A} as a function of n_A are shown in Fig. 7(right).) The saturation value decays exponentially with $n_{\bar{A}}$ for fixed n_A. **Middle:** We focus on the region with $n_A > n/2$, and contrast the non-monotonic time dependence with the monotonic behaviour for $n_A < n/2$ shown in left panel. The saturation value depends very weakly on $n_{\bar{A}}$ for fixed n_A, and we expect this weak dependence to go away in the thermodynamic limit. **Middle, inset:** We plot t^* (the time at which $F_A(t)$ is minimized, with $n_A > n/2$) for various n_A, n as a function of $n_{\bar{A}}$. Red/blue lines correspond to $n_A = 7, 8$. We find that $t^* \sim n_{\bar{A}}$, and does not depend on n_A. **Right:** We plot the dynamics of $F_A(t)$ with fixed $n = 12$ and various subsystem sizes.

3. To better understand the saturation value of $F_A(t)$ in unitary systems, we model the late-time state $|\psi(t)\rangle$ as a random pure state in the full Hilbert space drawn from the uniform (Haar) ensemble in Sec. 3.3. This calculation confirms the the universality of the scaling in (11).

Based on the expectation that the above results are universal, one particularly interesting example of a quantum chaotic system to which they should apply is a black hole. We discuss the implications of these results in the context of evaporating black holes in Sec. 3.4.

Before turning to specific models, let us discuss the general physical reasonableness of the results summarized above. Both the time-evolution and the saturation value of $F_A(t)$ for $n_A < n_{\bar{A}}$ is intuitive from the perspective of thermalization. In particular, the scaling $d_A/d_{\bar{A}}$ of the saturation value of $F_A(t)$ matches the expected scaling of the distance of the late-time state from the maximally mixed state, i.e., $\left(d_{\text{Bures}}\left(\rho_A(t), \frac{1}{d_A}\right)\right)^2 \sim d_A/d_{\bar{A}}$ [8, 38–40]. Note that the physical interpretation of the two quantities is somewhat different, and they did not necessarily have to show the same scaling based on kinematical reasoning: $F_A(t) = \left(\frac{d_{\text{Bures}}(\rho_A(t), \rho_A(t+dt))}{dt}\right)^2$ measures the *speed* of fluctuations, while $d_{\text{Bures}}\left(\rho_A(t), \frac{1}{d_A}\right)$ measures the absolute magnitude of fluctuations.

Perhaps the most striking feature of Fig. 1 is that for $n_A > n_{\bar{A}}$, we have an increasing behaviour of $F_A(t)$ at intermediate times, and an extensive late time-value. These behaviours cannot be understood purely from intuitions about thermalization, and require an understanding of new features of the dynamics of a unitary chaotic system.

We derive the result of non-monotonic time-evolution from numerical simulations in the chaotic spin chain in Sec. 3.1. To better understand its physical origin, recall that the reduced density matrix of $\rho_A(t)$ is not full-rank for $n_A > n_{\bar{A}}$. We can write the Hilbert space of A as a direct sum $\mathcal{H}_A = \mathcal{H}_{\text{ent}} \oplus \mathcal{H}_{\text{null}}$, where $\mathcal{H}_{\text{ent}}$ is the subspace spanned by the eigenstates of ρ_A with

non-zero eigenvalues, and $\mathcal{H}_{\text{null}}$ is the complementary subspace. Then we can divide $F_A(t)$ in (8) into two non-negative terms,

$$F_A(t) = F_{A,\text{ent}}(t) + F_{A,\text{rot}}(t) \tag{12}$$

where $F_{A,\text{ent}}(t)$ includes the terms in (8) where $|i\rangle, |j\rangle \in \mathcal{H}_{\text{ent}}$, while $F_{A,\text{rot}}(t)$ includes the terms where either $|i\rangle$ or $|j\rangle$ is in $\mathcal{H}_{\text{null}}$. Moreover, $F_{A,\text{rot}}(t)$ can be shown to be equal to

$$F_{A,\text{rot}}(t) = \text{Tr}\left[\rho_A \left(\frac{\mathrm{d}P_{\text{ent}}}{\mathrm{d}t}\right)^2\right] \tag{13}$$

where P_{ent} is the projector onto the subspace $\mathcal{H}_{\text{ent}}$. Note that no analog of this term is present in the the expression for $F_A(t)$ when $n_A \leq n/2$, as $F_A(t)$ quickly becomes full-rank in this case. On the other hand, if we take A to be the full system and consider a pure state, then $F_{A,\text{rot}}(t)$ is the only contribution to $F_A(t)$.

By considering the behaviour of $F_{A,\text{rot}}(t)$ and $F_{A,\text{ent}}(t)$ separately, we find that $F_{A,\text{ent}}(t)$ monotonically decays with time, while $F_{A,\text{rot}}(t)$ monotonically increases with time (see Fig. 5). The competition between these two terms leads to the non-monotonic evolution of $F_A(t)$.

$F_{A,\text{ent}}(t)$ is quantitatively close to $F_{\bar{A}}(t)$ in general, and the two can be shown to be equal in the case where the spectrum of ρ_A is flat (see around eq. (A.13) in Appendix A). $F_{A,\text{rot}}(t)$ is the dominant contribution to $F_A(t)$ at late times. Heuristically, its increasing behaviour captures the fact that the support of $\rho_A(t)$ gains access to more and more of full Hilbert space $\mathcal{H}_A$ to rotate within as time evolves. Eventually, it has access to the full Hilbert space of $\mathcal{H}_A$ and rotates at a large universal speed, leading to the extensive saturation value (see Fig. 2).

In Appendix C, we define a simple analytical toy model for the time-evolved state $|\psi(t)\rangle$ using the Brownian GUE Hamiltonian [41, 42], in which the eigenvectors of ρ_A for the larger subsystem A increasingly explore the full Hilbert space. We calculate $F_A(t)$ in this model, and find that the result qualitatively matches the increasing behavior in the spin chain model. The model is too simple to reproduce features coming from locality, such as the fact that $t^* \propto n_{\bar{A}}$, which should be better understood in future work.

3.1 Chaotic and integrable spin chains

Let us first study the behaviour of the subsystem QFI in the mixed-field Ising model:

$$H = \sum_i Z_i Z_{i+1} + g\sum_i X_i + h\sum_i Z_i \tag{14}$$

with periodic boundary conditions. For generic values of g and h, this model is chaotic by a variety of measures, including energy eigenvalue statistics [43], entanglement growth [22,44], and operator growth [45]. We take $g = -1.05$ and $h = 0.5$ as a standard representative of the chaotic case. The particular case where $h = 0$ is the integrable transverse field Ising model, which is integrable and can be written as a free fermion Hamiltonian.

We will consider the evolution of $F_A(t)$ for subsystem of contiguous spins of size n_A on a chain of length n. We take the initial states to be random product states between the different sites, for which the initial value of $F_A(t)$ is extensive in n_A. Such states are known to macroscopically equilibrate to infinite temperature [46]. We will average over samples drawn from the uniform measure on such states. The numerical results for $F_A(t)$ for the chaotic spin case are shown in Fig. 3, 4, and 5. Let us summarize the key features of these numerical results below.

For $n_A < n/2$, $F_A(t)$ shows a monotonic decay with t, which is of the form $F_A(t) \sim e^{-\alpha_{n_A}t}$ at intermediate times. The decay rate α_{n_A} decreases with increasing n_A, and is independent of
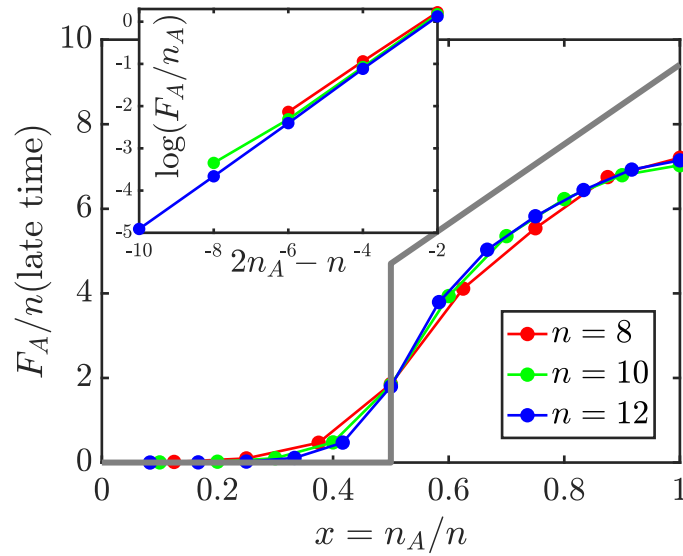
Figure 4: We plot the late time saturation value of $F_A(t)$ (averaged over 800 samples of initial states and 10 instances of time in the interval $t \in [15, 20]$) as a function of subsystem fraction $x \equiv n_A/n$, for various n. The solid grey line is the theoretical prediction from the random pure state model introduced in 3.3, in the thermodynamic limit $n \to \infty$. Even for finite size numerical results, we see a hint of a phase transition at $x = 1/2$. We expect based on the random pure state model that the result is likely to be extensive in n_A in the thermodynamic limit, which may be obscured by finite size effects here. **Inset:** Using the same data, we plot the log of the QFI saturation value for $x < 1/2$. We see a clear collapse as a function of $2n_A - n$ showing a scaling of $\sim d_A/d_{\bar{A}}$, as predicted in (20).
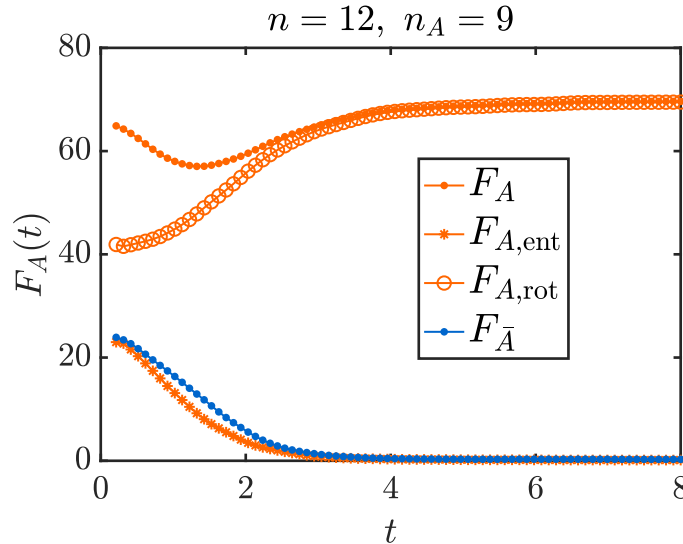

Figure 5: We plot the dynamics of $F_A(t), F_{\bar{A}}(t)$ for $n = 12, n_A = 9$ (averaged over 84 samples of initial random product states), along with the two terms $F_{A,\mathrm{ent}}$ and $F_{A,\mathrm{rot}}$ defined in (12). We observe that the non-monotonic behavior of $F_A(t)$ comes from the competition between $F_{A,\mathrm{ent}}(t)$ and $F_{A,\mathrm{rot}}(t)$.

359 $n_{\bar{A}}$. See Fig. 3 (left). The saturation value of $F_A(t)$ is proportional to $d_A/d_{\bar{A}} = 2^{2n_A - n}$, as shown
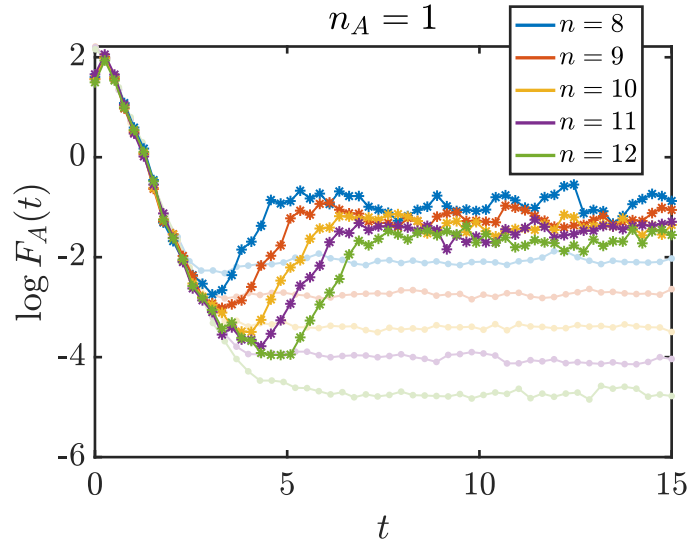360 more explicitly in Fig. 4.

Figure 6: We plot the dynamics of $F_A(t)$ from the integrable spin chain model for $n_A = 1$ and various full system sizes, averaged over 400 samples of initial random product states. For comparison, we also plot the $F_A(t)$ from the chaotic spin chain using the same but lighter colors. We observe that the time evolution coincides initially, but differs at later times. While the saturation value in the chaotic case decays exponentially with n for fixed n_A, the average value at late times in the integrable case is constant with respect to n.

For $n_A > n/2$, $F_A(t)$ shows an initial decay up to a time t^*. t^* depends only on $n_{\bar{A}}$, and is roughly proportional to $n_{\bar{A}}$. The fact that the behavior is qualitatively similar to the case $n_A < n/2$ up to this t^* physically makes sense, as it is only on this time scale that information from the larger system can travel across the smaller subsystem in the presence of local interactions. For $t > t^*$, $F_A(t)$ increases with time and later saturates. The saturation value is independent of $n_{\bar{A}}$ and grows with n_A, as shown in Fig. 4. [5]

In Fig. 5, we separately plot the two terms $F_{A,\text{rot}}$ and $F_{A,\text{ent}}$ defined below (12). We find that $F_{A,\text{ent}}(t)$ is both qualitatively and quantitatively close to $F_{\bar{A}}(t)$, and shows monotonic decay. $F_{A,\text{rot}}(t)$ monotonically grows, and fully accounts for the value of $F_A(t)$ at late enough times.

In the free-fermion integrable case of the spin chain model (14), where we set $h = 0$, we find strikingly different behavior of both the time-evolution and the saturation value of $F_A(t)$ for $n_A < n/2$ compared to the chaotiic case. See Fig. 6. These behaviours indicate that the state is far from equilibrating for the integrable model, even for a small subsystem. As shown in Fig. 6, the evolution with time is non-monotonic even for n_A much smaller than $n/2$. For both small and large n_A, the average late-time value saturation value is independent of $n_{\bar{A}}$, and grows with n_A. The time-evolution and saturation value of the QFI thus provides a sharp qualitative probe of the difference between chaotic and integrable systems.

3.2 Open quantum system with boundary dissipation

In this section, we consider an open system Lindbladian dynamics with boundary dissipation. For comparison with the results of the previous section, we call the number of sites in the full system n_A. The state $\rho(t)$ on the full system is evolved under a time-independent Lindbladian

---

[5]We find evidence for these statements up to finite-size corrections which make the data somewhat noisy. We will provide further evidence for various features using the models in Sec. 3.2 and Sec. 3.3, which are less affected by finite-size corrections.
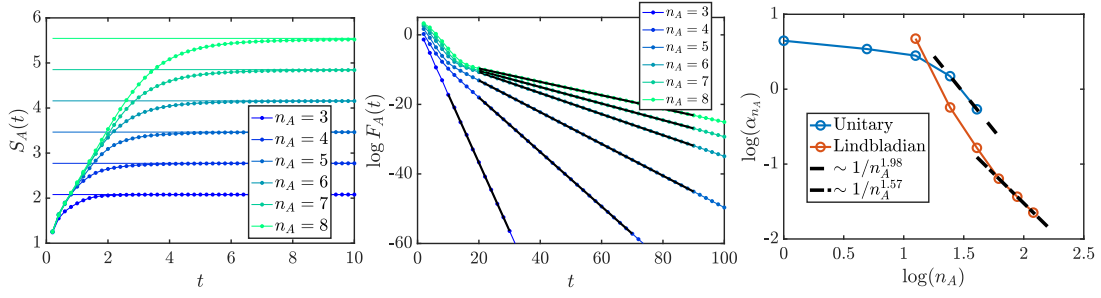
Figure 7: **Left:** The dynamics of the von Neumann entropy $S(t) = -\text{Tr}[\rho(t)\log\rho(t)]$ in the Lindbladian model, which shows a size-independent linear growth rate and saturation to $\log d_A$ at late times. These features resemble the behavior of a subsystem in the unitary model of Sec. 3.1. **Middle:** We plot the QFI dynamics in Lindbladian model, again starting from random initial states. The black solid lines show the fitting to the exponential decay rate. While we use the notation F_A, note that we are now considering different full system sizes n_A of the open quantum system. **Right:** We record the exponential decay rates α_{n_A} in both the unitary chaotic spin chain model of Sec. 3.1 and the non-unitary Lindbladian model. The decay rates α_{n_A} are obtained from fitting, as shown in the black solid lines in left panel of Fig. 7 and left panel of Fig. 3.

equation, which evolves the initial pure state to a mixed state:

$$
\begin{aligned}
\frac{\mathrm{d}}{\mathrm{d}t}\rho(t) &= \mathcal{L}(\rho(t)) \\
&= -i[H,\rho(t)] + \gamma\sum_a\left(L_a\rho(t)L_a^\dagger - \frac{1}{2}\{L_a^\dagger L_a, \rho(t)\}\right)
\end{aligned}
\tag{15}
$$

where $\{L_a\}$ is a set of jump operators and $\gamma \in \mathbb{R}_+$ controls the dissipation strength. We take H to be the same chaotic Ising Hamiltonian as (14), except now living on n_A sites and with open boundary conditions instead of periodic boundary conditions. We take the Lindblad operators $\{L_a\}$ to act on the two boundaries of the system, and make the arbitrary choice that the dissipation channel is the depolarization channel, with order one strength ($\gamma = 1$). Then the set of jump operators $\{L_a\}_{a=1}^6$ is specified as:

$$
\{L_a\}_{a=1}^6 = \{X_1, Y_1, Z_1, X_{n_A}, Y_{n_A}, Z_{n_A}\}
\tag{16}
$$

As a first check to get some intuition about this model, we show the dynamics of the von Neumann entropy of the state $\rho(t)$ on the full system in the right panel of Fig. 7. This matches the qualitative behavior of the entanglement entropy of a subsystem of a unitary chaotic spin chains very well [46]. It is thus natural to view this open system model as a way of extracting properties of the unitary system of Sec. 3.1 in the thermodynamic limit with $n_A \ll n$.

Under evolution by (15), $\rho(t)$ approaches the maximally mixed state in the following way:

$$
\rho(t) \approx \frac{\mathbf{1}}{d} + \rho_1 e^{-\lambda_1 t},
\tag{17}
$$

where $-\lambda_1$ is the eigenvalue of $\mathcal{L}(\cdot)$ with the least negative real part, and λ_1 is known as the Lindbladian gap. ρ_1 is some traceless operator. As the spectrum of $\rho(t)$ approaches that of a maximally mixed state, we can approximate $F(t) \approx d\,\text{Tr}(\dot{\rho}(t)^2)$ (here we apply the general formula (3)). Using (17), we find the exponential decay

$$
F(t) \sim e^{-2\lambda_1 t}.
\tag{18}
$$

14

399 In Ref. [47], the authors study the Lindbladian gap of a variety of one-dimensional chaotic
400 spin chain models with boundary dissipation, and find that it scales as $\lambda_1 \sim 1/n_A^\eta$, where $\eta \geq 1$
401 is some $\mathcal{O}(1)$ number. This universal behaviour of the Lindbladian gap thus naturally explains
402 our observation in Sec. 3.1 that the decay rate α_{n_A} decreases as we increase the system size
403 n_A.

404 For concreteness, in the left panel of Fig. 7, we show the QFI of $\rho(t)$ under such a Lindbla-
405 dian, and indeed find qualitatively the same behaviour of the QFI as in the previous subsection
406 on varying the system size n_A. In the right panel of Fig. 7, we plot the decay rate α_{n_A} as a func-
407 tion of n_A, and observe that it indeed scales in a power law fashion, with power larger than
408 one. The time evolution data is generated by Runge-Kutta method, and the decay rate from
409 fitting the data matches twice Lindbladian gap.

3.3 Random pure states

411 A useful model for the late-time state $|\psi(t)\rangle$ in a unitary chaotic evolution on a finite-dimensional
412 Hilbert space is a random pure state drawn from the uniform (Haar) ensemble. We will use
413 this state $|\psi_{\text{Haar}}\rangle$ to understand the saturation value of $F_A(t)$ at late times, ignoring the fact
414 that the state up to this point was evolved by the Hamiltonian H. We expect this approxima-
415 tion to be reasonable for states whose dynamics are not significantly constrained by the effects
416 of energy conservation.

417 More explicitly, we replace $e^{-iHt}\sigma_0 e^{iHt}$ in (8) with $|\psi_{\text{Haar}}\rangle\langle\psi_{\text{Haar}}|$, and the eigenvalues p_i
418 and eigenvectors $|i\rangle$ of $\sigma_A(t)$ with those of $\text{Tr}_{\bar{A}}|\psi_{\text{Haar}}\rangle\langle\psi_{\text{Haar}}|$, and then average over $|\psi_{\text{Haar}}\rangle$
419 in the full expression.

420 For this calculation, the general expressions for $F_A(t)$ of a pure state in terms of the Schmidt
421 decomposition in Appendix A will prove useful. To use these, we need to describe the ensemble
422 of Haar-random states in terms of their Schmidt decomposition, which is given as follows (here
423 we use S to refer to the smaller subsystem out of A and $\bar{A}$, and $\bar{S}$ to refer to its complement):

$$|\psi_{\text{Haar}}\rangle = \sum_{i=1}^{d_S} \sqrt{p_i}\,(V|i\rangle)_S\,(U|\tilde{i}\rangle)_{\bar{S}}\,. \tag{19}$$

424 The d_S real numbers p_i, the $d_S \times d_S$ unitary V, and the the $d_{\bar{S}} \times d_{\bar{S}}$ unitary U are random and
425 uncorrelated with each other. U and V are both Haar-random unitaries in their respective
426 Hilbert spaces. $\{|i\rangle\}$ and $\{|\tilde{i}\rangle\}$ are arbitrary fixed sets of d_S orthonormal states in S and $\bar{S}$
427 respectively. p_i have the statistics of the eigenvalues of normalized Wishart matrices $\frac{YY^\dagger}{\text{Tr}[YY^\dagger]}$,
428 where Y is a $d_S \times d_{\bar{S}}$ matrix of independent complex Gaussian random variables drawn from
429 the distribution $p(Y) = \mathcal{N}^{-1}e^{-d_{\bar{S}}\text{Tr}[YY^\dagger]}$. Using the expressions of Appendix A and (19), we
430 can write the expression for F_A in terms of averages of just second moments $U \otimes U^* \otimes U \otimes U^*$
431 of Haar-random unitaries U (similarly for V), so we get identical results for the more general
432 class of states where V and U are unitary 2-designs.

433 Let us decompose a general local Hamiltonian H as $H = H_A + H_{\bar{A}} + H_{\text{int}}$, where H_A consists
434 of all terms entirely within A, $H_{\bar{A}}$ of all terms entirely within $\bar{A}$, and H_{int} of all terms across the
435 boundary. Up to small corrections which can be ignored in the thermodynamic limit, we show
436 in Appendix B that (19) gives the following prediction for the late-time value of the subsystem
437 QFI:

$$F_A = \begin{cases} 2d_{\bar{A}}^{-1}\text{Tr}_A[H_A^2] = c\,n_A\,d_A/d_{\bar{A}} & n_A < n/2 \\ 4\text{Tr}_A[H_A^2]/d_A = 2c\,n_A & n_A > n/2 \end{cases} \tag{20}$$

438 where c is a constant of units energy density squared which depends on $\mathcal{O}(1)$ microscopic cou-
439 plings. This expression approximately reproduces the numerically observed late-time scaling
440 in the chaotic case of the spin chain model, as shown in Fig. 4. We do not find a quantitative

15

match between the two models, likely both due to finite size effects and due to the oversimplification in completely ignoring the effects of energy conservation by using (19).

The above result does not directly apply to initial states $|\psi_0\rangle$ which macroscopically resemble a finite temperature thermal density matrix $\rho_\beta = e^{-\beta H}/Z_\beta$ at late times. We expect that a natural generalization to such states, at least for sufficiently small β, should be given by

$$F_A = \begin{cases} 2(\langle H_A^2 \rangle_\beta - \langle H_A \rangle_\beta^2) e^{S_{A,\beta} - S_{\bar{A},\beta}} & S_{A,\beta} < S_{\bar{A},\beta} \\ 4(\langle H_A^2 \rangle_\beta - \langle H_A \rangle_\beta^2) & S_{A,\beta} > S_{\bar{A},\beta} \end{cases}. \tag{21}$$

where $S_{A,\beta}$ and $S_{\bar{A},\beta}$ are the thermodynamic entropies at inverse temperature β in A and $\bar{A}$, and $\langle \cdots \rangle_\beta$ indicates expectation values in ρ_β.

3.4 Evaporating black holes

If we assume that the formation of a black hole and its subsequent evaporation are governed by a unitary and chaotic evolution, the combined state of the black hole and its radiation can be seen as an example of $|\psi(t)\rangle$ at late times in a chaotic quantum many-body system. The simplest model for this combined state is a Haar-random pure state (19). Results from random pure states and their natural finite-temperature generalizations have previously been used to predict the Page curve for the entropy of the black hole and radiation in [11, 15], as well as the sudden recoverability of quantum information from the black hole radiation after the Page time in [12]. Here, we will apply this model in order to predict the behaviour of the subsystem QFI of the radiation for the time estimation task.

In the evaporating black hole setup, it is natural to consider the subsystem QFI of time estimation using the radiation. The time differences that we want to estimate are much smaller than the slow time scale on which the mass M of the black hole decreases due to emission of further radiation and correspondingly its Hawking temperature $T_H = 1/(8\pi G_N M)$ increases. That is, we are interested in time differences $\delta t \ll \delta t_{\text{evap}} \sim G_N M$. Hence, we can discuss the task of time estimation at a fixed M and T_H, where the number of degrees of freedom of the black hole and radiation are fixed. The Hamiltonian of the system has the form $H = H_B + H_R$ for some fixed H_B, H_R, and the state $|\psi(t)\rangle$ macroscopically resembles the thermal density matrix $e^{-\beta H_B} \otimes e^{-\beta H_R}/Z_B(\beta) Z_R(\beta)$ for fixed $\beta = 1/T_H$.

In this setup, we can apply our general formula (21). For this, we need to know the form of the energy variance $(\langle H_R^2 \rangle_\beta - \langle H_R \rangle_\beta^2)$ of the state $e^{-\beta H_R}/Z_R$. Let us model the radiation as a 1+1 dimensional photon gas, motivated by the fact that the emission into the low angular momentum modes is favored. For a (1+1)-D photon gas of one-dimensional volume L and temperature T, the expectation value of the energy is

$$\langle H_R \rangle_{\beta=1/T} \sim L T^2. \tag{22}$$

where $\sim$ indicates ignoring dimensionless constants, as we will continue to do in the remaining equations. The energy variance is then given by

$$\langle H_R^2 \rangle_\beta - \langle H_R \rangle_\beta^2 = T^2 \frac{\partial \langle H_R \rangle_{\beta=1/T}}{\partial T} \sim L T^3 \sim \frac{L}{(G_N M)^3} \tag{23}$$

where in the last expression we have put in $T = T_H$. Now let us treat the total evaporation time t_{evap} up to the current time as a proxy for the volume L of the photon gas. t_{evap} can be expressed in terms of the remaining black hole mass M (see for instance [15] or [48]), so that we have

$$L \sim t_{\text{evap}}(M) \sim G_N^2 (M_0^3 - M^3) \tag{24}$$

where M_0 is the initial mass of the black hole. We therefore find that the energy variance is given by

$$\langle H_R^2 \rangle_\beta - \langle H_R \rangle_\beta^2 \sim \frac{1}{G_N} \left(\frac{M_0^3}{M^3} - 1 \right) . \tag{25}$$

The quantity $\left(\frac{M_0^3}{M^3} - 1 \right)$ keeps track of the stage in the evaporation process and grows as more radiation is emitted.

Now using this expression in (21), we see that before the Page time, when $S_{B,\beta} - S_{R,\beta}$ is large, we have a very small value of the subsystem QFI of the radiation, $F_R \sim 1/G_N \mathcal{O}(e^{-1/G_N})$, which gives a time uncertainty of $\mathcal{O}(e^{1/G_N})$ (recall Eq. (2) for the relation between the Fisher information and the time uncertainty). Indeed, taking into account the slow evolution of the temperature of the radiation and assuming it can be simply measured gives us a better way of estimating the time in this case, with uncertainty $\sim \delta t_{\text{evap}} = G_N M$. On the other hand, after the Page time,

$$F_R \sim 1/G_N \left(\frac{M_0^3}{M^3} - 1 \right), \quad S_{R,\beta} > S_{B,\beta} . \tag{26}$$

The corresponding uncertainty $|\delta t|$ in time using the optimal quantum measurement on $\rho_R(t)$ is $\mathcal{O}(\sqrt{G_N})$, which is much smaller than the naive uncertainty best-case uncertainty of δt_{evap} based on Hawking's calculation. This is true as long as the black hole mass is much larger than the Planck mass ($M \gg 1/\sqrt{G_N}$), at which point the black hole evolves very rapidly in Hawking's calculation and the semiclassical analysis is even naively expected to break down. It would be interesting to see what new prescriptions may be needed to resolve this version of the information paradox and reproduce the behavior (26). See the discussion section Sec. 7 for more comments.

4 Classical fisher information for simple measurements

The analysis so far revealed that with optimal measurements on any subsystem larger than half, the uncertainty of the time estimation task in $|\psi(t)\rangle$ is suppressed as $1/n$, where n is the full system size. In particular, this is very different from the infinite uncertainty in an equilibrium state $\rho^{(\text{eq})}$. It is reasonable to expect, however, that the measurements needed to accurately estimate the time using more than half the system have a high computational complexity. This expectation would be particularly important in the context of the evaporating black hole setup of Sec. 3.4, as it would imply that computationally bounded observers would see results consistent with Hawking's state. Complexity-theoretic criteria for the validity of semiclassical gravity have previously been proposed in the context of other information-theoretic tasks, see for instance [20–25].

To address the question about the complexity of time estimation, recall from Sec. 2 that the optimal measurement basis (in which the uncertainty is given by the quantum Fisher information) is the eigenbasis of $\mathcal{R}_\rho^{-1}(\partial \rho / \partial t)$. For the full system, recall that there is a simple general expression given by (7). The resulting measurement basis is at least as complex as the state $|\psi(t)\rangle$ itself.

For a subsystem, we do not have a simple expression for the optimal measurement basis, but can find it numerically in examples like the chaotic spin chain by diagonalizing $\mathcal{R}_{\rho_A}^{-1}([\partial \rho_A / \partial t])$. While directly evaluating the computational complexity is beyond the scope of current techniques, we find that the entanglement entropy of typical states in the optimal measurement basis at late times is volume-law and close to the Page value. An example is shown in Fig 8. This tells us that the complexity of the measurement basis is at least proportional to the sub-system volume [49].
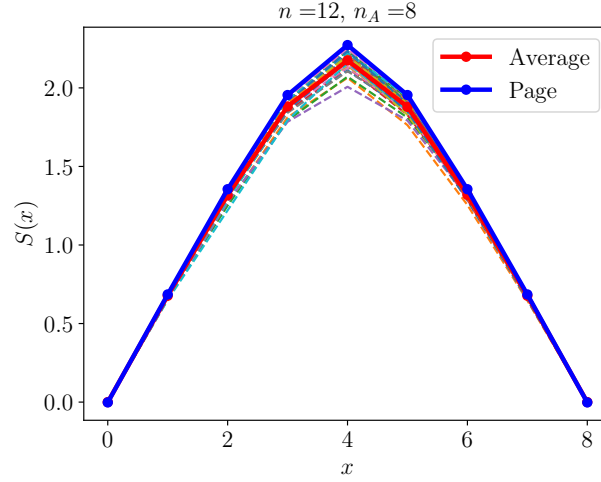
Figure 8: We evolve a single initial random product state in the chaotic spin chain (14) for $L = 12$ to $t = 10$, by which time we expect the QFI reaches its large saturation value (see Fig. 4). We pick $n_A = 8$, find the eigenstates of the operator $\mathcal{R}_{\rho_A}^{-1}(\partial \rho_A / \partial t)$, and show their entanglement entropies in arbitrarily chosen intervals of size x as a function of x. The entropies of individual eigenstates are shown with dashed lines, and their average is shown with a thick red curve. The blue curve is the Page value [11] for the corresponding system sizes.

A natural alternative setup is to restrict to *simple measurements* on a subsystem, and consider the classical Fisher information (CFI) associated with them (2). On making this restriction, do we get a small saturation value of the CFI even on considering a subsystem bigger than half of the system? The simplest measurements we can consider are in the computational basis (say, the eigenbasis of the Z operators at each site). Both from the chaotic spin chain and from the random pure state model (19), we find that the late-time saturation value of this CFI has the following behavior:

$$f_A^{\text{comp}}(t)_{\text{late times}} = \kappa \, \frac{n}{d_{\bar{A}}} \; . \tag{27}$$

where κ is a constant of units energy density squared which depends on microscopic couplings in the Hamiltonian. See Fig. 9 for the numerical spin chain result, and Appendix D for the random pure state calculation. Hence, as long as $n_A < n - \mathcal{O}(\log n)$, even for $n_A > n/2$, the late-time value of the f_A^{comp} is exponentially suppressed in n. The late-time value is therefore effectively indistinguishable from the zero result we would obtain from the equilibrium density matrix $\rho^{(\text{eq})}$, or equivalently from Hawking's state in the black hole context. Moreover, the numerical result of Fig. 9 (top) shows that the decay with time is monotonic in this regime, which is again intuitive from the perspective of thermalization.

What about the regime where the subsystem is so large that $n_{\bar{A}} \leq \mathcal{O}(\log n)$? In the evaporating black hole setup, this corresponds to very late times in the evaporation process where the black hole entropy is $\mathcal{O}(\log G_N)$. In this regime, the CFI is no longer exponentially suppressed, and in particular, if we take A to be the full system, the CFI is extensive in n (see Fig. 9 (bottom)). This tells us that it is possible to estimate time with high accuracy ($\mathcal{O}(1/n)$ variance) using measurements of $\mathcal{O}(1)$ complexity if we have access to the full system. The number of measurement outcomes needed is also likely to be $\mathcal{O}(1)$ or at worst polynomial in n. See the next section for some evidence for this using explicit experiments. In fact, as we will discuss in the next section, we can further use this simple procedure to distinguish the full
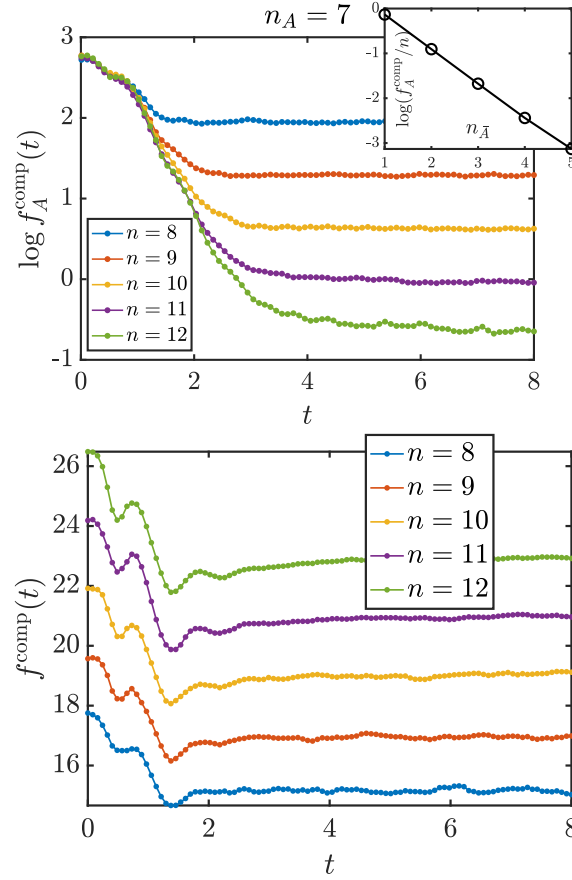
Figure 9: **Top:** Subsystem computational basis CFI f_A^{comp} for $n_A = 7$ and different full system sizes, starting from intial random product states and averaged over 400 samples. We see that there is an exponential decay of the saturation value with $n_{\bar{A}}$ for fixed n_A. This should be contrasted with the late-time result in Fig. 3 (middle) for $F_A(t)$, the Fisher information corresponding to optimal measurements, which is almost independent of $n_{\bar{A}}$. **Top, inset:** We plot the late-time saturation value of $f_A^{\text{comp}}(t)$ as a function of $n_{\bar{A}}$, and the scaling matches (27). **Bottom:** Full system computational basis CFI f^{comp} for different full system sizes. Both the initial and the final value are proportional to n.

544   state $|\psi(t)\rangle$ of the system from a thermal density matrix such as $\rho^{(\text{eq})}$.[6]

545   Note that we have assumed here that evaluating an estimator function $T_{\text{est}}(\xi_1, ..., \xi_N)$ on
546 the measurement outcomes which saturates the Cramer-Rao bound (2) is a simple process.
547 In particular, suppose we use the maximum likelihood estimate (MLE) discussed in the next
548 section. Then we can evaluate T_{est} efficiently if the form of $p_\xi(t) = \langle \xi | e^{-iHt} \sigma_0 e^{iHt} | \xi \rangle$ as a
549 function of time for each $\xi = 1, ..., 2^n$ in the computational basis is given to us as input. We
550 leave discussions of whether this additional resource is reasonable, and how complex it is
551 to actually evaluate $p_\xi(t)$, to future work. For now, we note that even with this additional
552 resource, if we are in the regime where $n_{\bar{A}} \geq \mathcal{O}(\log n)$, operations of $\mathcal{O}(1)$ circuit and sample
553 complexity that we have considered here cannot be used to estimate t or distinguish $|\psi(t)\rangle$
554 from $\rho^{(\text{eq})}$ at late times.

---

[6]There are other known ways of distinguishing $\text{Tr}_{\bar{A}}[|\psi(t)\rangle\langle\psi(t)|]$ from $\text{Tr}_{\bar{A}}\rho^{(\text{eq})}$ with $\mathcal{O}(\text{poly}(n))$ sample and circuit complexity when $n_{\bar{A}} \leq \mathcal{O}(\log(n))$, such as the SWAP test [9, 25, 50] which makes use of the large difference in second Renyi entropy between these states. See another example of a test that works in this regime in Section 5 of [22].

Regardless of the above somewhat intricate complexity-theoretic considerations, the large value of the computational basis CFI in the regime $n_{\bar{A}} \leq \mathcal{O}(\log n)$ indicates that the state $\text{Tr}_{\bar{A}}[|\psi(t)\rangle\langle\psi(t)|]$ is not thermalizing to a steady state in this regime, even from the perspective of simple measurements. It seems difficult to reconcile this statement with the fact that we expect (for instance based on the model of a Haar-random state) that the probability of any given measurement outcome for a simple measurement is exponentially close in n between $|\psi(t)\rangle$ and $\rho^{(\text{eq})}$, even on the full system (see for instance [21, 22]). To better understand how these statements can be consistent, we note that there is an $\mathcal{O}(1)$ total variation distance (trace distance) between the classical probability distribution in the computational basis associated with the late-time $|\psi(t)\rangle$ (modelled as a Haar-random state) and the uniform distribution [51]. [7] More explicitly, for the full system, we find that while the individual probability differences appearing in the trace distance are suppressed as $\mathcal{O}(e^{-n})$, the sum over exponentially many terms makes the trace distance $\mathcal{O}(1)$. Indeed, this result was previously used in [31] to deduce that the ability to estimate time using simple measurements on the full system is surprisingly good, using a different measure involving the classical mutual information. For a subsystem A, we find in Appendix E.2 that the total variation distance decays exponentially with $n_{\bar{A}}$. This confirms from a different perspective that the state $\text{Tr}_{\bar{A}}[|\psi(t)\rangle\langle\psi(t)|]$ equilibrates from the perspective of simple measurements in the regime $n_A \leq n - \mathcal{O}(\log n)$, but not necessarily for larger n_A.

5   An experiment on estimating time

The quantum and classical Fisher informations that we have calculated in various models in the previous sections indicate certain setups where we should in principle be able to accurately estimate t_0 using the time-evolved state $\rho(t_0)$. How would we carry out this process of time estimation in practice, using some set of measurement outcomes from the state? In this section, we will discuss an explicit estimator function called the maximum likelihood estimator (MLE), which is widely used in statistical inference. We will explicitly demonstrate its application for the task of time estimation in a quantum many-body system, by performing a numerical "experiment" in the spin chain model of Sec. 3.1.

The maximum likelihood estimate for the time estimation task is defined as follows. Recall that in our setup, the family of states $\rho(t)$ is given by either $e^{-iHt} |\psi_0\rangle\langle\psi_0| e^{iHt}$ or $\text{Tr}_{\bar{A}}[e^{-iHt} |\psi_0\rangle\langle\psi_0| e^{iHt}]$, and hence the measurement outcomes correspond to certain basis states $|\xi\rangle$ on either the full system or subsystem A. Given outcomes $\xi_1, ..., \xi_N$ from independent measurements on N copies of the state $\rho(t_0)$, the maximum likelihood estimate $T_{\text{ML}}(\xi_1, ..., \xi_N)$ can be found by evaluating the global maximum of the following log-likelihood function over t:

$$\ell(\xi_1, ..., \xi_N | t) = \sum_{i=1}^{N} \log p_{\xi_i}(t), \quad p_\xi(t) \equiv \langle\xi|\rho(t)|\xi\rangle . \tag{28}$$

If the form of $p_\xi(t)$ as a function of t for any outcome $|\xi\rangle$ is given to us as input, or can be computed numerically as we do in our "experiment" below, $T_{\text{ML}}(\xi_1, ..., \xi_N)$ can be evaluated in a straightforward way. On general grounds [32], for large N, the mean of $T_{\text{ML}}(\xi_1, ..., \xi_N)$ should approach the true underlying value t_0 of time, and its uncertainty $(\delta T_{\text{ML}})^2$ defined in (1) should saturate the Cramer-Rao bound (2).

In a quantum many-body system of volume n, a complete measurement of any extensive subsystem has $\mathcal{O}(e^n)$ possible outcomes. A potential concern may be that the sample size N needed for the Cramer-Rao bound to be saturated might itself grow rapidly with n. We will

---

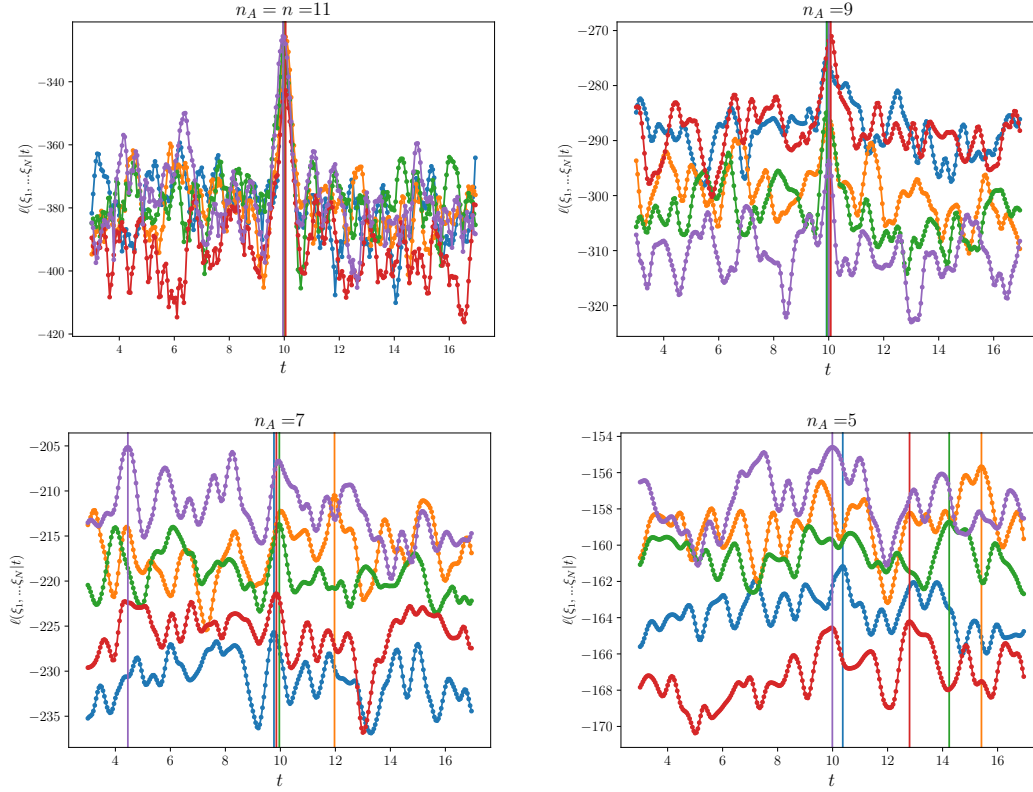[7]We present a self-contained derivation of this result using a resolvent technique in Appendix E.1.

Figure 10: We time-evolve a single instance of an initial random product state by the chaotic spin chain Hamiltonian up to time $t_0 = 10$. The full system size is taken to be $n = 11$, and we consider different values of $n_A = 11, 9, 7, 5$. In each case, we draw $N = 50$ samples in the computational basis and plot the log-likelihood function (28) based on these (and repeat the process 5 times). We see that the estimate T_{ML}, indicated with the vertical lines corresponding to the global maxima, is much more reliable in cases with a larger value of the classical Fisher information f_A^{comp}. By considering similar data for other full system sizes $n = 8, 9, 10$, the N needed for the estimate to become reliable does not appear to grow significantly with n: in particular, $N = 50$ used here is a small fraction of the 2048 states in the full Hilbert space in this case.

provide evidence using the spin chain experiment below that this is not the case, and individual realizations of T_{ML} for $\mathcal{O}(1)$ N are very close to t_0 in cases where the Fisher information is large.

Let us carry out some explicit (numerical) experiments to estimate time. We take the initial state $|\psi_0\rangle$ to be some arbitrary single choice of a random product state on system size $n = 11$. We numerically sample from the probability distribution of either the full time-evolved state $e^{-iHt_0}|\psi_0\rangle$, or its reduced density matrix on a subsystem A, in the computational basis using python. We use the Hamiltonian of the chaotic spin chain (14). We obtain N samples from this distribution, and plug these into (28) to obtain the log-likelihood function of t. In practice, we find this function by computing $p_{\xi_i}(t)$ for any given ξ_i as a function of t by numerically computing it for some finite set of times and interpolating. In Fig. 10, we show results from drawing $N = 50$ samples from the state at $t_0 = 10$ for various subsystem sizes, and repeating the experiment 5 times.

Recall from (27) that the late-time computational basis CFI f_A^{comp} is large for the full sys-

tem, and rapidly decreases for subsystems. Consistent with this, in the case of the full system (top left of Fig. 10), we find a very sharp maximum in the log-likelihood function close to $t = t_0$ for each repetition of the experiment. As we decrease the subsystem size, the local maximum close to t_0 becomes less sharp and the variance of its location increases. Note that in all cases, the log-likelihood function has a large number of other local maxima besides the global maximum in the range of times we consider. An interesting feature which we could not have predicted *a priori* is that in cases with large CFI, the global maximum always seems to be very close to the actual value of t_0. In cases where f_A^{comp} is small, picking the global maximum yields unreliable results.

We can now see how such an experiment can be used to distinguish the time-evolved state from the equilibrium density matrix. Suppose we are given an $\mathcal{O}(1)$ number of copies of a state which is either $\rho_A(t) = \text{Tr}_{\bar{A}}[e^{-iHt} |\psi_0\rangle\langle\psi_0| e^{iHt}]$ for some known $|\psi_0\rangle$ and H, or the equilibrium density matrix $\rho_A^{(\text{eq})} = \text{Tr}_{\bar{A}}[\rho^{(\text{eq})}]$. We do not know which of the two states we have, but are told from the Born rule what the functions $p_\xi(t)$ for each ξ would be as a function of t, if the state were $\rho_A(t)$. Suppose the computational basis CFI of $\rho_A(t)$ is large. Then one procedure that allows us to decide which state we have is to measure in the computational basis, and apply the MLE according to the state $\rho_A(t)$. We can repeat this experiment some $\mathcal{O}(1)$ number of times, as we do above in Fig. 10. If the variance in our resulting estimates of t is small and decreasing as $1/N$ with the sample size N, this indicates that the state we are measuring is indeed $\rho_A(t)$. If not, the state is $\rho_A^{(\text{eq})}$. This provides an efficient way of distinguishing $\rho_A(t)$ from $\rho_A^{(\text{eq})}$. In cases where the CFI of $\rho(t)$ is exponentially small in n, the difference between $\rho_A^{(\text{eq})}$ and $\rho_A(t)$ would likely become impossible to detect due to constraints of any reasonable experimental apparatus.
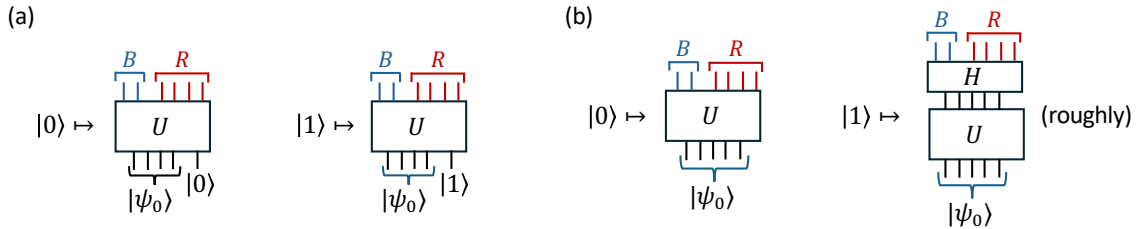

Figure 11: We compare the structure of the isometric encodings in the quantum error correcting code in the Hayden-Preskill protocol (a) and the one that appears naturally in the time estimation task (b). In both cases, U is time-evolution operator up to some late-time t in a chaotic system, which can for instance be modelled as a Haar-random unitary. (a) is a much more effective quantum error-correcting code than (b) as it makes use of the full scrambling power of the time-evolution operator to non-locally encode the information of the logical qubit.

6   Quantum error-correction perspective and comparison to Hayden-Preskill protocol

In this section, we discuss a further physical interpretation of the transition in the saturation value of $F_A(t)$ between less than half and more than half of the system, from the perspective of quantum error-correction. The sudden improvement in our ability to estimate time using more than half of the system is reminiscent of the sudden improvement in the ability to recover information in the Hayden-Preskill protocol [12]. To compare the two tasks more directly, in

this section we will analyse the question about inferring the value of time in the language of quantum error-correction.

The quantum error-correction task we consider was introduced in [29]. [8] Let us motivate it as follows. The information of interest, which we want to encode and recover, is whether the time is t or $t + dt$. Say that the logical $|0\rangle$ state corresponds to time t, and the logical $|1\rangle$ state to $t + dt$. Intuitively, this logical information is encoded in the quantum many-body system via the following map:

$$|0\rangle \to |\psi(t)\rangle, \quad |1\rangle \to |\psi(t + dt)\rangle . \tag{29}$$

This map is not quite suitable for setting up a quantum error-correcting code, as it is not an isometry due to the non-orthogonality of $|\psi(t)\rangle$ and $|\psi(t + dt)\rangle$. Note that the normalized state along the component of $|\psi(t + dt)\rangle$ that is orthogonal to $|\psi(t)\rangle$ is $|\xi(t)\rangle$ defined in (7). Hence, a natural choice of an isometry to replace the map (29) is:

$$|0\rangle \mapsto |\psi(t)\rangle, \quad |1\rangle \mapsto |\xi(t)\rangle . \tag{30}$$

This is an encoding of one logical qubit into the n physical qubits of our quantum many-body system. Now suppose we want to correct for erasure errors on some subsystem B (which represents the black hole in the black hole evaporation setup). Can we recover the logical information from the remaining subsystem R?

Faist et al [29] found a relation between the QFI and a weaker variant of the Knill-Laflamme conditions for the above error-correcting code as follows. In our notation, they showed that if the QFI of the subsystem R, $F_R(t)$, is equal to the QFI of the full system, then their Knill-Laflamme condition is exactly satisfied. Hence, if there is no sensitivity loss in metrology on tracing out subsystems, the code is perfectly error-correctable (in the weaker sense of [29]). In the present physical setup, we find that the subsystem QFI $F_R(t)$ is always smaller than the full system QFI $F(t)$. This motivates us to ask about the approximate error-correcting properties of the code (30). Specifically, we would like to see if the error-correction works better in the regime where the subsystem QFI is extensive (even though it is not as large as the full system QFI), and poorly in the regime where the subsystem QFI is exponentially small.

A good test for error correctability of a logical qubit is to examine the distinguishability of two orthogonal codewords under noise. In particular, let us consider the late-time regime, in which $|\psi(t)\rangle$ can be modelled by $|\psi_{\text{Haar}}\rangle$ in (19), and $|\xi\rangle$ is still defined according to (7) for the particular choice our many-body Hamiltonian H. We would like to see how well $\rho_R \equiv \text{Tr}_B[|\psi\rangle\langle\psi|]$ and $\sigma_R \equiv \text{Tr}_B[|\xi\rangle\langle\xi|]$ can be distinguished.

We use Holevo's just-as-good fidelity $F_H(\rho, \sigma) \equiv \text{Tr}[\sqrt{\rho}\sqrt{\sigma}]$ as the distinguishability measure.[9] We find that the noisy codewords are indistinguishable for less than half of the system, and the fidelity improves linearly for more than half of the system (see Appendix F for details):

$$F_H(\rho_R, \sigma_R) \approx \begin{cases} 1 & d_R < d_B \\ \frac{n_B}{n} & d_R > d_B \end{cases} . \tag{31}$$

This result qualitatively matches the behavior (20) that we found for the QFI.

In the Hayden-Preskill protocol, the isometric encoding of the quantum error-correcting code is as shown in Fig. 11(a). In this case, the output states corresponding to any two orthogonal input states become perfectly distinguishable on any subsystem larger than half of the system, i.e., the information becomes perfectly recoverable just after the Page time. In (31), the states ρ_R and σ_R do not become perfectly distinguishable just after the Page time,

---

[8]Also see [52] for a related quantum error-correction task and its holographic description.

[9]This measure is easier to evaluate than the fidelity, and it is "just as good" because it also satisfies the Fuchs–van de Graaf inequalities, $1 - F_H(\rho, \sigma) \leq \frac{1}{2}||\rho - \sigma||_1 \leq \sqrt{1 - F_H(\rho, \sigma)^2}$.

but there is a sudden improvement in their distinguishability after the Page time: the fidelity drops from 1 to 1/2. Comparing the structure of the isometric encodings in the two codes in Fig. 11, we see that the two codes make use of the scrambling time-evolution operator in a different way, and in particular, the code in the Hayden-Preskill case uses the full power of the scrambling evolution to non-locally encode the logical information, while the code (30) does not.

7 Conclusions and Discussion

In this paper, we used an operational question about time-estimation to probe new features of the dynamics of quantum many-body systems and black holes. We found an interesting interplay between thermalization and unitarity in the quantum Fisher information which determines the uncertainty of the optimal time estimate. For a small subsystem, we found a sharp distinction between integrable and chaotic systems in terms of this quantity. Further, we understood its non-monotonic evolution for a subsystem larger than half of the system in terms of the rapid rotation of the support of the reduced density matrix in the full Hilbert space. We found a version of the black hole information loss paradox in terms of the failure of Hawking's naive calculation in semiclassical gravity to agree with general predictions for this quantity based on unitarity. We further studied how the behaviour of the classical Fisher information associated with simple measurements is consistent with expectations from coarse-grained properties of thermalization in chaotic many-body systems. Moreover, the Fisher information with this restriction on complexity also matches expectations based on semiclassical gravity in the black hole context.

There are a number of interesting directions for future work related to general quantum many-body systems, black holes, and complexity theory, which we summarize in the three sections below.

7.1 Questions about quantum many-body systems

An interesting feature of the QFI for time estimation compared to other information-theoretic quantities that have been studied previously is that it involves the relation between the time-evolved state and the Hamiltonian in a crucial way. While we have focused on the class of effectively "infinite-temperature" initial pure states and emphasized what the QFI is telling us about their entanglement properties such as their Schmidt vectors, it is important to note that the QFI is not simply a measure of entanglement. For example, $F_A(t)$ is zero in any subsystem for any energy eigenstate of the system, although typical eigenstates are highly entangled. An important question for future work is to understand the behaviour of this quantity for initial states whose dynamics are more strongly constrained by energy conservation, such as initial states in a microcanonical window, and to understand the interplay between information and energy dynamics in this setting. The equilibrium approximation of [53] should provide a useful tool for addressing this question.

It would be interesting to see if some version of the QFI can be calculated in random models of local unitary chaotic systems such as random unitary circuits [54, 55], which are analytically tractable for computing certain quantities such as the Renyi entropies. It would also be interesting to see if the QFI can be related to other quantities that capture universal aspects of chaos, such as OTOCs. A particularly natural set of quantities that may be related to the QFI would be the time-evolved circuit complexity [6] and Krylov complexity of the state [56], which naturally involve distance metrics between nearby states. It would be important to come up with a definition of mixed-state complexity that is appropriate for comparison to the subsystem QFI [57–59].

726   We found that the subsystem QFI is a useful way of detecting the difference between chaotic
727 and free-fermion integrable systems. It would be interesting to also consider the behavior
728 of this quantity in interacting integrable systems like the Heisenberg model or many-body
729 localized systems [60]. Other interesting cases would be ones that are intermediate between
730 integrable and chaotic, such as systems with Hilbert space fragmentation and quantum many-
731 body scars [61].

7.2   Questions about black holes

733 One main question we pose about black holes is how the prediction (26) that the subsytem
734 QFI of the radiation is $\mathcal{O}(1)$ after the Page time can be reproduced with a gravity calculation.
735 Recent results on obtaining the Page curve from gravity calculations [16–19] made use of the
736 AdS/CFT correspondence, and in particular of prescriptions for calculating the entanglement
737 entropy of the boundary theory using bulk quantities [62–65].
738   Finding a bulk dual of the quantum Fisher information in order to set up a similar calcu-
739 lation would require some further work. From (5), the QFI is related to the Bures distance,
740 or equivalently the fidelity between the states at t and $t + dt$. The fidelity is the exponent
741 of the Renyi-$\frac{1}{2}$ relative entropy, which may not have a simple semiclassical gravity dual. von
742 Neumann entropic quantities such as the relative entropy are better understood as having
743 semiclassical gravity duals [66, 67]. Hence, for the purpose of understanding QFI in the bulk,
744 it may be more appropriate to study a variant of the QFI, known as the Boguliubov-Kubo-Mori
745 QFI [68, 69], that is based on the gradient of the relative entropy. This quantity may provide
746 a better starting point for exploring the physical phenomena we have identified through the
747 QFI in gravity. From preliminary numerical studies, we have found that this quantity behaves
748 in a qualitatively similar way to the QFI in quantum many-body systems.
749   Prior works [70–73] have explored the relevance of the Fisher information metric in grav-
750 ity, but the dynamics of QFI associated with time estimation have not yet been analyzed. As-
751 suming that one could find a bulk dual of the QFI or some other related quantity, another
752 interesting setup to apply it to in gravity would be a quantum quench in the boundary CFT,
753 which corresponds to black hole formation in the bulk [74–76]. In particular, it would be very
754 interesting to see if such a calculation could reproduce the increasing behaviour of the larger
755 subsystem QFI at intermediate times, see Fig. 1.

7.3   Questions about complexity

757 In the regime where $n/2 < n_A < n - \mathcal{O}(\log(n))$, it is often believed that it is exponentially
758 hard to distinguish $\text{Tr}_{\bar{A}}[|\psi(t)\rangle\langle\psi(t)|]$ from $\text{Tr}_{\bar{A}}[\rho^{(\text{eq})}]$. This exponential hardness has been
759 particularly important in the evaporating black hole example, as it implies that observers with
760 bounded computational complexity will not be able to detect that the fundamental description
761 of quantum gravity is distinct from semiclassical effective field theory [20–25]. Our results
762 imply that observers who have the ability to measure the QFI of ρ_R after the Page time, and
763 hence see that it has an extensive value instead of the zero value for $\rho_R^{(\text{eq})}$, can tell the difference
764 between semiclassical gravity and the fundamental description.
765   Is measuring the subsystem QFI in the regime $n/2 < n_A < n - \mathcal{O}(\log(n))$ provably an
766 exponentially hard task? If so, is it hard because making the measurement in the optimal basis
767 is itself exponentially complex, or because implementing the maximum likelihood estimate on
768 the measurement outcomes is exponentially complex? Our results on entanglement entropy
769 of the measurement basis (Fig. 8) lower-bound its computational complexity as $C \geq \mathcal{O}(n)$, but
770 determining whether or not the complexity is exponential in n would be an important question
771 for future work.

We stress that the statement we want to make here is about the difficulty of distinguishing $\rho^{(\text{eq})}$ from a known one-parameter family of states $\rho_A(t)$. This is likely a stronger statement than the one commonly studied in the complexity theory literature, where the state ρ_A to be distinguished from $\rho^{(\text{eq})}$ is randomly sampled from an ensemble [9, 50, 77]. While some hardness results are proved and argued in the case where ρ_A is drawn from an ensemble [9, 78], there is no known rigorous hardness result for our setting. Together with the evidence and arguments from [22, 24, 25, 77], our results motivate a further investigation of this complexity-theoretic question that is vital to the validity of semiclassical physics.

In this paper, we have worked out the QFI for the optimal measurement basis and the CFI for the simple computational basis, and found that they show sharply different behaviors. It would also be interesting to calculate the CFI for other computationally efficient measurement bases, and see how much the CFI can improve by using a circuit of polynomial depth before measuring.

It would also be interesting to perform the experiment of Sec. 5 to estimate the time in an actual lab setting, making use of recent progress in simulating quantum many-body dynamics with a large number of degrees of freedom (see for instance [79]). This would allow us to check if the sample complexity for the time estimation task is indeed $\mathcal{O}(1)$ in a quantum many-body system. It is likely the hardest step in these cases may be to evaluate the classical probabilities $p_\xi(t)$ of Sec. 5 as a function of t in order to perform the MLE. An important ingredient of this effort would then be to find an efficient way to evaluate these probabilities, or to see if it is provably difficult to do so.

A   Subsystem QFI in terms of Schmidt decomposition

In this appendix, we will further analyze the general formula for the subsystem quantum Fisher information $F_A(t)$ from (8) for the case where the global state $|\psi(t)\rangle$ is pure. Let us rewrite (8) here for the pure state case for clarity:

$$F_A(t) = \sum_{\substack{i,j \text{ s.t.} \\ p_i+p_j \neq 0}} \frac{2}{p_i+p_j} |\langle i|\text{Tr}_{\bar{A}}[H, |\psi(t)\rangle\langle\psi(t)|]|j\rangle|^2 \tag{A.1}$$

where $p_i, |i\rangle$ are eigenvalues and eigenstates of $\text{Tr}_{\bar{A}}[|\psi(t)\rangle\langle\psi(t)|]$. Recall that we have suppressed the t-dependence of $p_i, |i\rangle$ in the notation. We will further drop the t label in $|\psi(t)\rangle$ for most of the remaining discussion to simplify notation. It is useful to divide (A.1) into the following terms:

$$F_A = 2F_{A,+} - F_{A,-} - (F_{A,-})^* \tag{A.2}$$

810 where

$$F_{A,+} = \sum_{\substack{1 \le j,k \le \min(d_A, d_{\bar{A}}) \\ p_j + p_k \ne 0}} \frac{2}{p_j + p_k} \langle j| \text{Tr}_{\bar{A}}[H |\psi\rangle\langle\psi|]|k\rangle \, \langle k|\text{Tr}_{\bar{A}}[|\psi\rangle\langle\psi|H]|j\rangle \, , \tag{A.3}$$

$$F_{A,-} = \sum_{\substack{1 \le j,k \le \min(d_A, d_{\bar{A}}) \\ p_j + p_k \ne 0}} \frac{2}{p_j + p_k} \langle j| \text{Tr}_{\bar{A}}[H |\psi\rangle\langle\psi|]|k\rangle \, \langle k|\text{Tr}_{\bar{A}}[H |\psi\rangle\langle\psi|]|j\rangle \, . \tag{A.4}$$

811 To avoid repeatedly using $\min(d_A, d_{\bar{A}})$, let us refer to S as the smaller subsystem and B as its
812 complement in the remaining discussion. The Schmidt decomposition of $|\psi\rangle$ can be expressed
813 as:

$$|\psi\rangle = \sum_{a=1}^{d_S} \sqrt{p_a} \, |\psi_a\rangle_S |\phi_a\rangle_B \, . \tag{A.5}$$

814 We can take the Schmidt vectors $|\phi_a\rangle$, $a = 1,...,d_S$ to be the first d_S basis vectors of an
815 orthonormal basis for subsystem B, and the remaining basis vectors can be labelled $|\phi_a\rangle$,
816 $a = d_S + 1,...,d_B$. These remaining $|\phi_a\rangle$'s are the zero eigenvectors of ρ_B, which should
817 also be included in the sums (A.3) and (A.4) when we take $A = B$. We can also extend the set
818 of p_i to include i from $i = d_S + 1$ to $i = d_B$, setting all p_i in this range to zero. We will not
819 put explicit S and B subscripts on the Schmidt vectors in the rest of the discussion: the $|\psi_a\rangle$'s
820 always live in S and $|\phi_a\rangle$'s in B.
821 Now consider the expression for $F_{S,+}$, taking $A = S$ in (A.3). Using the Schmidt decompo-
822 sition (A.5), we can write

$$\langle \psi_j| \text{Tr}_B[H |\psi\rangle\langle\psi|]|\psi_k\rangle = \sqrt{p_k} \, \langle\psi_j| \langle\phi_k| H |\psi\rangle \, . \tag{A.6}$$

823 Putting this into the expression for $F_{S,+}$, and assuming that all p_i for i from 1 to d_S are non-zero,
824 we find

$$F_{S,+} = \sum_{j=1}^{d_S} \sum_{k=1}^{d_S} \frac{2p_k}{p_j + p_k} \langle\psi_j| \langle\phi_k| H |\psi\rangle \, \langle\psi| H |\psi_j\rangle |\phi_k\rangle \, , \tag{A.7}$$

$$= \sum_{j=1}^{d_S} \sum_{k=1}^{d_B} \frac{2p_k}{p_j + p_k} \langle\psi_j| \langle\phi_k| H |\psi\rangle \, \langle\psi| H |\psi_j\rangle |\phi_k\rangle \tag{A.8}$$

825 where we have used that p_k from $k = d_S + 1$ to $k = d_B$ are zero. We can similarly express $F_{B,+}$
826 in terms of the Schmidt coefficients and vectors:

$$F_{B,+} = \sum_{j=1}^{d_S} \sum_{k=1}^{d_B} \frac{2p_j}{p_j + p_k} \langle\psi_j| \langle\phi_k| H |\psi\rangle \, \langle\psi| H |\psi_j\rangle |\phi_k\rangle \, . \tag{A.9}$$

827 Putting (A.8) and (A.9) together, we therefore have

$$F_{S,+} + F_{B,+} = 2 \sum_{j=1}^{d_S} \sum_{k=1}^{d_B} \langle\psi| H |\psi_j\rangle |\phi_k\rangle \, \langle\psi_j| \langle\phi_k| H |\psi\rangle = 2 \langle\psi|H^2|\psi\rangle \, . \tag{A.10}$$

828 Note that for $|\psi\rangle = |\psi(t)\rangle = e^{-iHt} |\psi\rangle$, (A.10) is independent of t. Hence,

$$F_{S,+}(t) + F_{B,+}(t) = 2 \langle\psi_0|H^2|\psi_0\rangle \, . \tag{A.11}$$

27

829   Next, consider $F_{A,-}$. Again by using the Schmidt decomposition of $|\psi\rangle$, one can check that

$$F_{S,-}(t) = F_{B,-}(t) = \sum_{j=1}^{d_S} \sum_{k=1}^{d_S} \frac{2\sqrt{p_j}\sqrt{p_k}}{p_j + p_k} \langle\psi| H |\psi_j\rangle |\phi_k\rangle \langle\psi| H |\psi_k\rangle |\phi_j\rangle \; . \tag{A.12}$$

830   We further notice that $F_S = F_{B,\text{ent}}$ when S and B are maximally entangled in $|\psi(t)\rangle$. ($F_{B,\text{ent}}$
831   is defined below (12).) To show this, we first note that:

$$\begin{aligned}
F_{B,\text{ent}}(t) &= \sum_{\substack{i,j \text{ s.t.} \\ p_i \neq 0, p_j \neq 0}} \frac{2}{p_i + p_j} |\langle i| \text{Tr}_S [H, |\psi(t)\rangle\langle\psi(t)|] |j\rangle|^2 \\
&= \sum_{j=1}^{d_S} \sum_{k=1}^{d_S} \frac{2p_j}{p_j + p_k} \langle\psi_j| \langle\phi_k| H |\psi\rangle \langle\psi| H |\psi_j\rangle |\phi_k\rangle - F_{B,-} - F_{B,-}^*
\end{aligned} \tag{A.13}$$

832   The first term of above equation only sums over non-zero eigenvalues, so it is different from
833    $F_{B,+}$, but similar to $F_{S,+}$ (see (A.7) for comparison). In particular, when the spectrum is flat
834   ($p_k = p_j$), the first term equals $F_{S,+}$. Then using the fact that $F_{B,-} = F_{S,-}$, (A.13) becomes
835   equal to F_S.
836   (A.7), (A.11), and (A.12) will be useful for our later calculations. The structure of (A.11)
837   and (A.12) is interesting. While the term $F_{A,-}$ is equal for subsystems $A = S$ and $A = B$ (similar
838   to quantities like entanglement entropy) at all times, $F_{A,+}$ suggests that there is some tradeoff
839   between S and B in the time-evolution.
840   Consistent with the idea of such a tradeoff, we note as an interesting aside that (A.11) and
841   (A.12) together are equivalent to a certain "time-energy uncertainty relation" found in [29].
842   This is an uncertainty relation that quantifies a trade-off between the fluctuations in time mea-
843   surements and the fluctuations in energy measurements. We briefly review it in the remaining
844   part of this section.
845   Any uncertainty relation involves a pair of conjugate variables. In [29], the authors iden-
846   tified a variable η conjugate to t that is generated by the optimal local time measurement
847   operator T. As explained in [29], the theory of quantum fisher information gives us a formula
848   for the optimal operator T that measures the time close to t and minimizes the variance of the
849   time estimation on the full system,

$$T = t + \frac{1}{F(t)} \sum_{i,j} \frac{2}{p_i + p_j} \langle i| [H, |\psi\rangle\langle\psi|] |j\rangle |i\rangle\langle j| \; . \tag{A.14}$$

850   Consider now a conjugate variable η that is defined via an evolution generated by T,

$$\partial_\eta |\psi(\eta)\rangle\langle\psi| = i[T, |\psi\rangle\langle\psi|] \; . \tag{A.15}$$

851   We consider infinitesimal flows in the η direction, so the state $|\psi\rangle\langle\psi|$ appearing on the RHS of
852   (A.15) is the same as the one that appears in (A.14). It is shown that the optimal operator to
853   measure η, analogous to the operator (A.14) for measuring t, simply equals the Hamiltonian.
854   Hence, the parameter η can be seen as the total energy of the system.
855   Now we consider the problem of estimating the total energy of the system by performing
856   the measurement on a subsystem. Let $\rho_{A\bar{A}}(t, \eta)$ be the pure state on $A\bar{A}$ (we return to the
857   notation $A\bar{A}$ to indicate that A can be either the smaller or the larger subsystem). We are
858   interested in the variances of estimations of t and η on subsystems A and $\bar{A}$ respectively. We
859   denote corresponding the QFI of the full system by $F(t)$ and $F(\eta)$ respectively. [29] first show
860   that on the full system, the QFI $F(\eta)$ of the state under the flow by (A.15) is determined by
861   the QFI $F(t)$ under the flow of t as follows:

$$F(\eta) = 4/F(t) = 1/(\langle H^2\rangle_{\psi_0} - \langle H\rangle_{\psi_0}^2) \; . \tag{A.16}$$

862 Next, just as we can consider the flow by t for the reduced density matrices of a subsystem,
863 we can do the same for the flow by η and consider the subsystem QFI $F_{\bar{A}}(\eta)$. [29] then find
864 the following time-energy uncertainty relation for subsystems:

$$\frac{F_A(t)}{F(t)} + \frac{F_{\bar{A}}(\eta)}{F(\eta)} = 1 \ . \tag{A.17}$$

865 where using (A.15), $F_{\bar{A}}(\eta)$ is given by the following formula:

$$\begin{aligned}
F_{\bar{A}}(\eta) &= \frac{1}{4(\langle H^2 \rangle_{\psi_0} - \langle H \rangle_{\psi_0}^2)} \sum_{\substack{i,j \text{ s.t.} \\ p_i + p_j \neq 0}} \frac{2}{p_i + p_j} |\langle i| \mathrm{Tr}_S \{H - \langle H \rangle_{\psi_0}, |\psi\rangle\langle\psi|\} |j\rangle|^2 \ , \\
&= \frac{4}{F(t)^2} \left(2F_{\bar{A},+}(t) + F_{\bar{A},-}(t) + F_{\bar{A},-}(t)^*\right) \ .
\end{aligned} \tag{A.18}$$

866 where the second line follows from the same decomposition of (A.2) after changing the com-
867 mutator to the anticommutator.

868   Note that the above equation involves an anticommutator inside the trace. The result (A.17)
869 says that the better one can estimate the evolution time t of the full system from a subsystem,
870 the worse one can estimate the energy η of the full system from the complementary subsystem,
871 and vice versa.

872   Let us now show the uncertainty relation (A.17) is equivalent to our (A.11) and (A.12).
873 For simplicity, we assume w.l.o.g. that $\langle H \rangle_{\psi_0} = 0$. Then (A.11) is equivalent to

$$2F_{A,+}(t) + 2F_{\bar{A},+}(t) = F(t) \ , \tag{A.19}$$

874 and (A.18) is equivalent to

$$\begin{aligned}
F_{\bar{A}}(\eta) &= \frac{1}{4 \langle H^2 \rangle_{\psi_0}} \sum_{\substack{i,j \text{ s.t.} \\ p_i + p_j \neq 0}} \frac{2}{p_i + p_j} |\langle i| \mathrm{Tr}_S \{H, |\psi\rangle\langle\psi|\} |j\rangle|^2 \ , \\
&= \frac{4}{F(t)^2} \left(2F_{\bar{A},+}(t) + F_{\bar{A},-}(t) + F_{\bar{A},-}(t)^*\right) \ .
\end{aligned} \tag{A.20}$$

875   Adding and subtracting $F_{A,-}(t)$ gives

$$2F_{A,+}(t) - F_{A,-}(t) - F_{A,-}(t)^* + 2F_{\bar{A},+}(t) + F_{A,-}(t) + F_{A,-}(t)^* = F(t) \ . \tag{A.21}$$

876 Using (A.12),

$$2F_{A,+}(t) - F_{A,-}(t) - F_{A,-}(t)^* + 2F_{\bar{A},+}(t) + F_{\bar{A},-}(t) + F_{\bar{A},-}(t)^* = F(t) \ . \tag{A.22}$$

877 Dividing both sides by $F(t)$, we have

$$\frac{F_A(t)}{F(t)} + \frac{2F_{\bar{A},+}(t) + F_{\bar{A},-}(t) + F_{\bar{A},-}(t)^*}{F(t)} = \frac{F_A(t)}{F(t)} + \frac{2F_{\bar{A},+}(t) + F_{\bar{A},-}(t) + F_{\bar{A},-}(t)^*}{F(t)^2 F(\eta)/4} = \frac{F_A(t)}{F(t)} + \frac{F_{\bar{A}}(\eta)}{F(\eta)} = 1 \ , \tag{A.23}$$

878 where the first equality uses $F(t)F(\eta) = 4$ and the second equality uses (A.20). This is the
879 uncertainty relation (A.17).

B Subsystem QFI for random pure states

In this Appendix, we will give a derivation for (20). We will always use S to denote the subsystem smaller than half of the full system, and B to denote its complement. Recall the Schmidt decomposition of a random pure state from (19), which we repeat here for convenience:

$$|\psi\rangle = \sum_{i=1}^{d_S} \sqrt{p_i} \, (V |i\rangle)_S \, (U |\tilde{i}\rangle)_B \, . \tag{B.1}$$

We take the d_S real numbers p_i, the $d_S \times d_S$ unitary V, and the the $d_B \times d_B$ unitary U to be random and uncorrelated with each other. U and V are both Haar-random unitaries in their respective Hilbert spaces. $\{|i\rangle\}$ and $\{|\tilde{i}\rangle\}$ are arbitrary fixed sets of d_S orthonormal states in S and B respectively. p_i have the statistics of the eigenvalues of normalized Wishart matrices $\frac{YY^\dagger}{\text{Tr}[YY^\dagger]}$, where Y is a $d_S \times d_B$ matrix of independent complex Gaussian random variables drawn from the distribution $p(Y) = \mathcal{N}^{-1} e^{-d_B \text{Tr}[YY^\dagger]}$. In this appendix, we will use overlines to indicate all averages.

Let us first evaluate $F_{S,+}$ using (A.7). For any given realization of (B.1), we have

$$
\begin{aligned}
F_{S,+} &= \sum_{j,k,a,b=1}^{d_S} \frac{2p_k}{p_j + p_k} \sqrt{p_a} \sqrt{p_b} \, \langle \psi_j | \langle \phi_k | H | \psi_a \rangle | \phi_a \rangle \langle \psi_b | \langle \phi_b | H | \psi_j \rangle | \phi_k \rangle \\
&= \sum_{j,k,a,b=1}^{d_S} \frac{2p_k \sqrt{p_a p_b}}{p_j + p_k} \sum_{\substack{\alpha_1,\alpha_2, \\ \alpha_3,\alpha_4=1}}^{d_S} \sum_{\substack{\beta_1,\beta_2, \\ \beta_3,\beta_4=1}}^{d_B} \langle \alpha_1 | \langle \beta_1 | H | \alpha_2 \rangle | \beta_2 \rangle \langle \alpha_3 | \langle \beta_3 | H | \alpha_4 \rangle | \beta_4 \rangle \times V_{j\alpha_1} V_{a\alpha_2}^* V_{b\alpha_3} V_{j\alpha_4}^* \\
&\qquad\qquad\qquad\qquad\qquad\qquad\qquad\qquad\qquad\qquad\qquad\qquad\qquad \times U_{k\beta_1} U_{a\beta_2}^* U_{b\beta_3} U_{k\beta_4}^* \, . \tag{B.2}
\end{aligned}
$$

We have the following rules for the Haar averages:

$$
\begin{aligned}
&\overline{V_{j\alpha_1} V_{a\alpha_2}^* V_{b\alpha_3} V_{j\alpha_4}^*} \\
&= \frac{1}{d_S^2 - 1} \left(\delta_{aj} \delta_{jb} \delta_{\alpha_1\alpha_2} \delta_{\alpha_3\alpha_4} + \delta_{jj} \delta_{ab} \delta_{\alpha_1\alpha_4} \delta_{\alpha_3\alpha_2} - \frac{1}{d_S} (\delta_{aj} \delta_{jb} \delta_{\alpha_1\alpha_4} \delta_{\alpha_2\alpha_3} + \delta_{jj} \delta_{ab} \delta_{\alpha_1\alpha_2} \delta_{\alpha_3\alpha_4}) \right),
\end{aligned} \tag{B.3}
$$

$$
\begin{aligned}
&\overline{U_{k\beta_1} U_{a\beta_2}^* U_{b\beta_3} U_{k\beta_4}^*} \\
&= \frac{1}{d_B^2 - 1} \left(\delta_{ka} \delta_{kb} \delta_{\beta_1\beta_2} \delta_{\beta_3\beta_4} + \delta_{kk} \delta_{ab} \delta_{\beta_1\beta_4} \delta_{\beta_3\beta_2} - \frac{1}{d_B} (\delta_{ka} \delta_{kb} \delta_{\beta_1\beta_4} \delta_{\beta_3\beta_2} + \delta_{kk} \delta_{ab} \delta_{\beta_1\beta_2} \delta_{\beta_3\beta_4}) \right).
\end{aligned} \tag{B.4}
$$

For $F_{S,-}$, we have

$$
\begin{aligned}
F_{S,-} &= \sum_{j,k,a,b=1}^{d_S} \frac{2\sqrt{p_k} \sqrt{p_j}}{p_j + p_k} \sqrt{p_a} \sqrt{p_b} \, \langle \psi_a | \langle \phi_a | H | \psi_k \rangle | \phi_j \rangle \langle \psi_b | \langle \phi_b | H | \psi_j \rangle | \phi_k \rangle \\
&= \sum_{j,k,a,b=1}^{d_S} \frac{2\sqrt{p_k p_j p_a p_b}}{p_j + p_k} \sum_{\substack{\alpha_1,\alpha_2, \\ \alpha_3,\alpha_4=1}}^{d_S} \sum_{\substack{\beta_1,\beta_2, \\ \beta_3,\beta_4=1}}^{d_B} \langle \alpha_2 | \langle \beta_2 | H | \alpha_1 \rangle | \beta_1 \rangle \langle \alpha_3 | \langle \beta_3 | H | \alpha_4 \rangle | \beta_4 \rangle \\
&\qquad\qquad\qquad\qquad\qquad\qquad\qquad \times V_{a\alpha_2} V_{k\alpha_1}^* V_{b\alpha_3} V_{j\alpha_4}^* \times U_{a\beta_2} U_{j\beta_1}^* U_{b\beta_3} U_{k\beta_4}^* \, . \tag{B.5}
\end{aligned}
$$

Using the averages over U and V, we find

$$\overline{F_{S,+}} = \frac{\text{Tr}[H^2]}{(d_S^2-1)(d_B^2-1)}\left[(d_S^{-1}-d_B^{-1})\frac{I}{4}+(d_S^2-1)(1-d_S^{-1}d_B^{-1})\right]$$
$$+\frac{\text{Tr}[H]^2}{(d_S^2-1)(d_B^2-1)}\left[(-d_S^{-1}+d_B^{-1})\frac{I}{4}\right]$$
$$+\frac{\text{Tr}_B[(\text{Tr}_S H)^2]}{(d_S^2-1)(d_B^2-1)}\left[(-1+d_S^{-1}d_B^{-1})\frac{I}{4}\right]$$
$$+\frac{\text{Tr}_S[(\text{Tr}_B H)^2]}{(d_S^2-1)(d_B^2-1)}\left[(1-d_S^{-1}d_B^{-1})\frac{I}{4}+(d_S^2-1)(d_S^{-1}-d_B^{-1})\right] \tag{B.6}$$

and

$$\overline{F_{S,-}} = \frac{\text{Tr}[H^2]}{(d_S^2-1)(d_B^2-1)}\left[(d_S^{-1}+d_B^{-1})\frac{I}{4}+(d_S^2-1)(-d_S^{-1}d_B^{-1})\right]$$
$$+\frac{\text{Tr}[H]^2}{(d_S^2-1)(d_B^2-1)}\left[(d_S^{-1}+d_B^{-1})\frac{I}{4}+(d_S^2-1)(-d_S^{-1}d_B^{-1})\right]$$
$$+\frac{\text{Tr}_B[(\text{Tr}_S H)^2]}{(d_S^2-1)(d_B^2-1)}\left[(-1-d_S^{-1}d_B^{-1})\frac{I}{4}+(d_S^2-1)(d_S^{-1})\right]$$
$$+\frac{\text{Tr}_S[(\text{Tr}_B H)^2]}{(d_S^2-1)(d_B^2-1)}\left[(-1-d_S^{-1}d_B^{-1})\frac{I}{4}+(d_S^2-1)(d_S^{-1})\right] \tag{B.7}$$

where

$$I = \overline{\sum_{j,k=1}^{d_S}\frac{2(p_j-p_k)^2}{p_j+p_k}} \tag{B.8}$$

Altogether, using $\overline{F_S} = 2\overline{F_{S,+}} - 2\overline{F_{S,-}}$, we obtain:

$$\overline{F_S} = \frac{2}{(d_B^2-1)}\left(\text{Tr}[H^2]+\frac{1}{d_S d_B}\text{Tr}[H]^2-\frac{1}{d_S}\text{Tr}_B[(\text{Tr}_S H)^2]-\frac{1}{d_B}\text{Tr}_S[(\text{Tr}_B H)^2]\right) \tag{B.9}$$

$$+\frac{I}{(d_S^2-1)(d_B^2-1)}\left(-\frac{1}{d_B}\text{Tr}[H^2]-\frac{1}{d_S}\text{Tr}[H]^2+\frac{1}{d_S d_B}\text{Tr}_B[(\text{Tr}_S H)^2]+\text{Tr}_S[(\text{Tr}_B H)^2]\right) \tag{B.10}$$

$$\equiv F_S^{\text{flat}} + F_S^{\text{non-flat}} \tag{B.11}$$

where F_S^{flat} and $F_S^{\text{non-flat}}$ are defined in (B.9) and (B.10) respectively. The motivation for these definitions is that if we assume that the Schmidt spectrum is flat ($p_j = d_S^{-1}$ for each j), we have $F_S^{\text{non-flat}} = 0$ and $\overline{F_S} = F_S^{\text{flat}}$ as a consequence of $I = 0$.

Now, we want to estimate the magnitude of F_S in the limit $d_B \gg d_S \gg 1$. We further assume that H is a sum of traceless local terms, and write it as

$$H = H_S + H_B + H_{\text{int}} \tag{B.12}$$

where H_S and H_B include all terms contained within S and B respectively.

We first estimate the magnitude of F_S^{flat}. We notice that if $H_{\text{int}} = 0$, we have precisely $F_S^{\text{flat}} = 0$. The leading term in F_S^{flat} is quadratic in H_{int}:

$$F_S^{\text{flat}} = \frac{1}{d_B^2-1}\text{Tr}[H_{\text{int}}^2] \sim \frac{d_S^2}{d}\times\mathcal{O}(|\partial S|) \tag{B.13}$$

where $|\partial S|$ is the number of degrees of freedom involved in H_{int}, and is proportional to the area of the boundary of S for a local Hamiltonian. Next, we estimate the magnitude of $F_S^{\text{non-flat}}$, by first evaluating integral I. Define $\mu(x)$ as the normalized density distribution of the Schmidt spectrum:

$$\mu(x) = \frac{1}{d_S} \sum_{i=1}^{d_S} \delta(x - p_i) \tag{B.14}$$

Then I can be expressed as follows:

$$I = d_S^2 \int \mathrm{d}x\mathrm{d}y \langle \mu(x)\mu(y) \rangle \frac{2(x-y)^2}{x+y} \tag{B.15}$$

Here we can decompose the correlators $\langle \mu(x)\mu(y) \rangle$ into disconnected and connected parts. The disconnected part is built from $\langle \mu(x) \rangle$, which is the Marchenko-Pastur distribution and is approximately $\delta(x - 1/d_S)$ up to a small width of $\mathcal{O}(1/\sqrt{d})$. Since we are in the limit $d_B \gg d_S \gg 1$, we can safely ignore the level repulsion of the eigenvalues (which gives the connected part of the correlator), and approximate $\langle \mu(x)\mu(y) \rangle \approx \langle \mu(x) \rangle \langle \mu(y) \rangle$. The average density of the MP distribution is given by:

$$\langle \mu(x) \rangle = \frac{d_B}{2\pi} x^{-1} \sqrt{(x - x_-)(x_+ - x)}, \ x_- < x < x_+ \tag{B.16}$$

with the edge of the spectrum given by:

$$x_\pm = d_S^{-1} \left(1 \pm d_S^{1/2} d_B^{-1/2} \right)^2 \approx d_S^{-1} \pm 2d^{-1/2}. \tag{B.17}$$

In the limit $d_B \gg d_S \gg 1$, the MP distribution is a semi-circle centered at $x_c \equiv d_S^{-1}$ with width $\Delta \equiv 2d^{-1/2}$. Since the width is small, we can make the approximation $\frac{2(x-y)^2}{xy(x+y)} \approx \frac{2(x-y)^2}{2x_c^3}$. We then obtain:

$$\begin{aligned} I &\approx d_S^2 \left(\frac{d_B}{2\pi} \right)^2 \frac{1}{2(d_S^{-1})^3} \times \int_{-\Delta}^{\Delta} \mathrm{d}x\mathrm{d}y \ 2(x-y)^2 \sqrt{(\Delta^2 - x^2)(\Delta^2 - y^2)} \\ &= d_S^2 \left(\frac{d_B}{2\pi} \right)^2 \frac{1}{2(d_S^{-1})^3} \times \frac{\pi^2}{4} \Delta^6 \\ &= 2d_S^2 / d_B \end{aligned} \tag{B.18}$$

Now we are ready to estimate $F_S^{\text{non-flat}}$. First notice that in contrast to F_S^{flat}, $F_S^{\text{non-flat}}$ does not equal zero when $H_{\text{int}} = 0$. So to calculate the leading order contribution of $F_S^{\text{non-flat}}$, we can safely take $H_{\text{int}} = 0$. In this case, we obtain:

$$F_S^{\text{non-flat}} = \frac{\text{Tr}_S[H_S^2]}{d_S^2 - 1} I \approx 2d_B^{-1} \text{Tr}_S[H_S^2] \sim \frac{d_S^2}{d} \times \mathcal{O}(n_S) \tag{B.19}$$

Comparing (B.13) and (B.19), we find that they have the same $\sim \frac{d_S^2}{d}$ leading scaling, but with coefficients of the exponential part that are proportional to the area and volume of S respectively. Since we have a local Hamiltonian H, we should have $|\partial S| \ll n_S$. So the leading contribution to F_S comes from $F_S^{\text{non-flat}}$:

$$F_S \approx F_S^{\text{non-flat}} \approx 2d_B^{-1} \text{Tr}_S[H_S^2] \sim \frac{d_S^2}{d} \times \mathcal{O}(n_S) \tag{B.20}$$

Next, let us evaluate $\overline{F_B}$ for the larger subsystem B. We use the relations (A.10) and (A.12) to get

$$\overline{F_{B,+}} = 2\overline{\langle\psi|H^2|\psi\rangle} - \overline{F_{S,+}} = \frac{2}{d}\text{Tr}[H^2] - \overline{F_{S,+}} \quad , \quad \overline{F_{B,-}} = \overline{F_{S,-}} \tag{B.21}$$

So, we obtain:

$$\overline{F_B} = 4\overline{\langle\psi|H^2|\psi\rangle} - 2\overline{F_{S,+}} - 2\overline{F_{S,-}} \equiv F_B^{\text{flat}} + F_B^{\text{non-flat}} \tag{B.22}$$

where like in (B.11), $F_B^{\text{non-flat}}$ is the part of F_B proportional to I and F_B^{flat} is the remaining contribution.

First, we estimate the magnitude of F_S^{flat}. Given that the Hamiltonian is a sum of traceless local terms, we have the following scaling of the different traces:

$$\text{Tr}[H^2] \sim n\,d, \quad \text{Tr}_S[(\text{Tr}_B H)^2] \sim n_S d_B^2 d_S, \quad \text{Tr}_B[(\text{Tr}_S H)^2] \sim n_S d_S^2 d_B. \tag{B.23}$$

From this scaling, up to exponentially small contributions,

$$F_B^{\text{flat}} = 2\left(\frac{2}{d}\text{Tr}[H^2] - \frac{2}{d_B^2 d_S}\text{Tr}_S[(\text{Tr}_B H)^2]\right) \sim n_B. \tag{B.24}$$

Next, we estimate the magnitude of $F_B^{\text{non-flat}}$. $F_B^{\text{non-flat}}$ is given by:

$$F_B^{\text{non-flat}} = \frac{I}{(d_S^2-1)(d_B^2-1)}\left(-\frac{1}{d_S}\text{Tr}[H^2] - \frac{1}{d_B}\text{Tr}[H]^2 + \text{Tr}_B[(\text{Tr}_S H)^2] + \frac{1}{d_S d_B}\text{Tr}_S[(\text{Tr}_B H)^2]\right) \tag{B.25}$$

In the limit $d_B \gg d_S \gg 1$ and for a local Hamiltonian, we can drop the H_{int} term, and obtain:

$$F_B^{\text{non-flat}} \approx \frac{\text{Tr}_B[H_B^2]}{d_B^2-1}I \sim \frac{d_S^2}{d_B^2} \times \mathcal{O}(n_B) \tag{B.26}$$

Comparing with (B.24), we find that $F_B^{\text{non-flat}}$ is much more subleading. As a result, we obtain the magnitude of $\overline{F_B}$ as:

$$\overline{F_B} \approx F_B^{\text{flat}} \sim n_B \tag{B.27}$$

(B.20) and (B.27) together give our result in (20). We note that up to the volume-law vs. area law behaviour of the coefficient of the exponentially small value of F_S, the same result could have been obtained using the following models with a flat entanglement spectrum (as long as $H_{\text{int}} \neq 0$):

$$|\psi_{\text{flat}}\rangle = \sum_{i=1}^{d_S} d_S^{-1/2} V|i\rangle_S \otimes U|\tilde{i}\rangle_B. \tag{B.28}$$

or more simply,

$$|\psi_{\text{flat}}'\rangle = \sum_{i=1}^{d_S} d_S^{-1/2}|i\rangle_S \otimes U|\tilde{i}\rangle_B. \tag{B.29}$$

where $\{|i\rangle_S\}$ is an arbitrary basis for S, $\{|\tilde{i}\rangle_B\}$ is an arbitrary set of d_S orthonormal states in B, and U, V are Haar-random unitaries. We will sometimes use these models to simplify later calculations.

C A Brownian GUE toy model for the late-time state

This Appendix is motivated by our observation in Fig. 5 that the key reason for the growth of the QFI $F_B(t)$ at late times is the rotation of the support of $\rho_B(t)$ in $\mathcal{H}_B$. (Like in previous appendices, we will use S to denote the smaller subsystem and B to denote the larger subsystem.) Why does the speed of rotation, $F_{B,\text{rot}}$ from (13), grow with time? Intuitively, this result seems to be telling us that as the eigenbasis of ρ_B becomes more and more complicated and approaches a random subspace of $\mathcal{H}_B$, it is also able to change faster as a function of time on being slightly perturbed by the Hamiltonian. To check this intuition, we consider a model for the time-evolved state where by construction, the eigenbasis of ρ_B is becoming increasingly complicated with time:

$$|\psi(t)\rangle = \sum_{i=1}^{d_S} d_S^{-1/2} V|i\rangle_S \otimes U_{\text{aux}}(t)|\tilde{\psi}_i\rangle_B \,. \tag{C.1}$$

where V is a Haar-random unitary, and $U_{\text{aux}}(t)$ is the time-evolution operator associated with a time-dependent Hamiltonian with Brownian type disorder:

$$U_{\text{aux}}(t) = \mathcal{P}\exp\left[i\int_0^t dt' H_{\text{aux}}(t')\right], \tag{C.2}$$

$$\overline{H_{\text{aux},ij}(t)H_{\text{aux},kl}(t')} = d_B^{-1}\delta_{il}\delta_{jk}\delta(t-t'), \;\; i,j,k,l = 1,...,d_B \,. \tag{C.3}$$

Here, $H_{\text{aux}}(t)$ is a $d_B \times d_B$ matrix. This model, called Brownian Gaussian Unitary Ensemble (BGUE), was developed and extensively studied in [41, 42]. Since the dynamics of the eigenvalues of $\rho_{S,B}$ do not play an important role in the phenomenon we are interested in, we set them all equal to $1/d_S$, corresponding to the maximally mixed state on S.

Our goal is to understand explicitly whether, as the eigenbasis of ρ_B becomes more and more complicated in this model, it also evolves more rapidly on perturbation by a fixed local chaotic Hamiltonian H like that of the spin chain (14). We therefore evaluate the subsystem QFI of this time-evolved state (C.1) on further infinitesimal evolution by the original Hamiltonian H. Hence, in the formula (8), we replace $e^{-iHt}\sigma_0 e^{iHt}$ in (8) with $|\psi(t)\rangle\langle\psi(t)|$, and replace $p_i, |i\rangle$ with the eigenvalues and eigenvalues of $\text{Tr}_S[|\psi(t)\rangle\langle\psi(t)|]$, but use the Hamiltonian H from (14).

The advantage of using the model (C.1) is that it is analytically tractable. The averaged $F_A(t)$ of (C.1) only involves the first and second moment of the $U_{\text{aux}}(t)$ ensemble:

$$\overline{U_{\text{aux}}(t) \otimes U_{\text{aux}}^*(t)}, \quad \overline{U_{\text{aux}}(t) \otimes U_{\text{aux}}(t) \otimes U_{\text{aux}}^*(t) \otimes U_{\text{aux}}^*(t)} \tag{C.4}$$

which is exactly solvable with analytical results [42]. Note that the ensemble of BGUE saturates to the Haar random ensemble at $t \to +\infty$ [42], giving us the results from $|\psi_{\text{flat}}\rangle$ defined in (B.28) in the $t \to \infty$ limit. This model is too simple to incorporate any effects of locality, but will allow us to see that even without locality, it takes some $O(1)$ amount of time for the speed of rotation of $\rho_B(t)$ to reach its saturation value.

Having understood the motivations for the BGUE toy model, let us specify what to calculate. We eventually want to obtain $\overline{F_S(t)}, \overline{F_B(t)}, \overline{F_{B,\text{ent}}(t)}, \overline{F_{B,\text{rot}}(t)}$. Using conclusions from Appendix A, we have:

$$\overline{F_S(t)} = 2\overline{F_{S,+}(t)} - 2\overline{F_{S,-}(t)}, \quad \overline{F_B(t)} = 2\overline{F_{B,+}(t)} - 2\overline{F_{B,-}(t)}, \tag{C.5}$$

$$\text{with:} \;\; 2\overline{F_{S,+}(t)} + 2\overline{F_{B,+}(t)} = 4\overline{\langle\psi(t)|H^2|\psi(t)\rangle}, \quad \overline{F_{S,-}(t)} = \overline{F_{B,-}(t)} \tag{C.6}$$
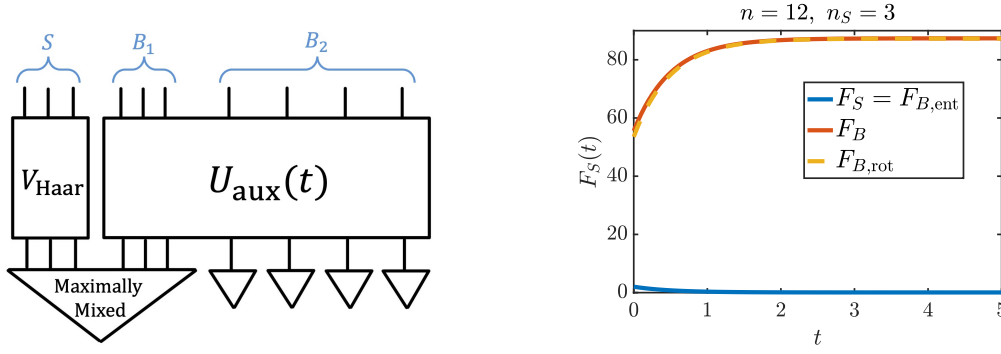
Figure 12: **Left:** An illustration of the time-dependent toy model defined in (C.1) and (C.14). **Right:** Dynamics of QFI in BGUE toy model.

where we used the fact that $\overline{F_{S,-}(t)}, \overline{F_{B,-}(t)}$ are real numbers. Specifying the Schmit spectrum to be maximally mixed, we further obtain additional constraints:

$$2\overline{F_{B,+}(t)} = \overline{F_{B,\text{rot}}(t)} + 2\overline{F_{S,+}(t)} \,. \tag{C.7}$$

Therefore, we only need to calculate three independent variables $\overline{F_{S,+}(t)}, \overline{F_{S,-}(t)}, \overline{\langle\psi(t)|H^2|\psi(t)\rangle}$, and then we can obtain everything else: $\overline{F_{B,\text{ent}}(t)} = \overline{F_S(t)} = 2\overline{F_{S,+}(t)} - 2\overline{F_{S,-}(t)}$, $\overline{F_{B,\text{rot}}} = 4\overline{\langle\psi(t)|H^2|\psi(t)\rangle} - 4\overline{F_{S,+}(t)}$

The derivation of $\overline{F_{S,+}(t)}, \overline{F_{S,-}(t)}, \overline{\langle\psi(t)|H^2|\psi(t)\rangle}$ essentially uses the technique developed in [42], with analytical result of first and second moment of BGUE ensemble as a function of time. Since the technical details are a bit involved, we only report the results.

We first define some intermediate variables for notational simplicity. First, denote:

$$P_B \equiv P_{\text{ent},0} = \sum_{i=1}^{d_S} (|\tilde{\psi}_i\rangle\langle\tilde{\psi}_i|)_B \tag{C.8}$$

where $|\tilde{\psi}_i\rangle_B$ are defined in (C.1). Therefore, P_B is the projector of subspace in $\mathcal{H}_B$ that is entangled with S at $t = 0$. Next, we define a set of intermediate variables $\{g_a\}_{a=1}^{12}$:

$$g_1 = \text{Tr}[H^2], \ g_2 = \text{Tr}[H^2 P_B], \ g_3 = \text{Tr}_S[(\text{Tr}_B[P_B H])^2], \ g_4 = \text{Tr}[(P_B H)^2],$$
$$g_5 = \text{Tr}_S[\text{Tr}_B[P_B H]\text{Tr}_B[H]], g_6 = \text{Tr}_S[(\text{Tr}_B[H])^2], \ g_7 = \text{Tr}_B[(\text{Tr}_S[H])^2], \ g_8 = \text{Tr}_B[P_B(\text{Tr}_S[H])^2],$$
$$g_9 = (\text{Tr}[P_B H])^2, \ g_{10} = \text{Tr}_B[(P_B\text{Tr}_S[H])^2], \ g_{11} = \text{Tr}[P_B H]\text{Tr}[H], g_{12} = (\text{Tr}H)^2 \,, \tag{C.9}$$

where H is the original chaotic Ising model Hamiltonian.

We further define another set of intermediate variables $\{f_b(t)\}_{b=1}^8$ [42]:

$$\begin{pmatrix} f_1(t) \\ f_2(t) \\ f_3(t) \\ f_4(t) \\ f_5(t) \\ f_6(t) \\ f_7(t) \\ f_8(t) \end{pmatrix} = \begin{pmatrix} 0 & 0 & \frac{1}{4} & \frac{1}{2} & \frac{1}{4} \\ 0 & \frac{d_B^2-2}{d_B(d_B^2-4)} & \frac{-1}{4(d_B-2)} & \frac{-1}{2d_B} & \frac{-1}{4(d_B+2)} \\ 0 & 0 & -\frac{1}{4} & 0 & \frac{1}{4} \\ 0 & \frac{-1}{d_B^2-4} & \frac{1}{4(d_B-2)} & 0 & \frac{-1}{4(d_B+2)} \\ \frac{1}{d_B^2-1} & \frac{-2}{d_B^2-4} & \frac{1}{2(d_B-1)(d_B-2)} & 0 & \frac{1}{2(d_B+1)(d_B+2)} \\ 0 & 0 & \frac{1}{4} & -\frac{1}{2} & \frac{1}{4} \\ \frac{-1}{d_B^3-d_B} & \frac{4}{d_B(d_B^2-4)} & \frac{-1}{2(d_B-1)(d_B-2)} & 0 & \frac{1}{2(d_B+1)(d_B+2)} \\ 0 & \frac{2}{d_B(d_B^2-4)} & \frac{-1}{4(d_B-2)} & \frac{1}{2d_B} & \frac{-1}{4(d_B+2)} \end{pmatrix} \times \begin{pmatrix} 1 \\ e^{-t} \\ e^{-(2-2d_B^{-1})t} \\ e^{-2t} \\ e^{-(2+2d_B^{-1})t} \end{pmatrix} \tag{C.10}$$

We finally obtain:

$$\overline{F_{S,+}(t)} = (d_S^{-2}g_4)f_1(t) + (2d_S^{-1}g_2 + 2d_S^{-2}g_5)f_2(t) + (2d_S - 2g_3)f_3(t) + (4d_S^{-2}g_2 + 4d_S^{-1}g_5)f_4(t)$$
$$+ (g_1 + d_S^{-1}g_6)f_5(t) + (d_S^{-2}g_4)f_6(t) + (d_S^{-1}g_1 + g_6)f_7(t) + (2d_S^{-1}g_2 + 2d_S^{-2}g_5)f_8(t) \tag{C.11}$$

For $\overline{F_{S,-}(t)}$, we further define $\alpha = d_S^{-1}\frac{1}{d_S^2-1}, \beta = d_S^{-1}\frac{-1}{d_S^3-d_S}$, then we find:

$$\overline{F_{S,-}(t)} = (\alpha g_3 + \beta g_4 + \beta g_9 + \alpha g_{10})f_1(t) + (2d_S^{-2}g_5 + 2d_S^{-2}g_8)f_2(t)$$
$$+ (2\beta g_3 + 2\alpha g_4 + 2\alpha g_9 + 2\beta g_{10})f_3(t) + (4d_S^{-2}g_2 + 4d_S^{-2}g_{11})f_4(t)$$
$$+ (d_S^{-1}g_6 + d_S^{-1}g_7)f_5(t) + (\alpha g_3 + \beta g_4 + \beta g_9 + \alpha g_{10})f_6(t)$$
$$+ (d_S^{-1}g_1 + d_S^{-1}g_{12})f_7(t) + (2d_S^{-2}g_5 + 2d_S^{-2}g_8)f_8(t) \,. \tag{C.12}$$

For $\overline{\langle\psi(t)|H^2|\psi(t)\rangle}$, we obtain:

$$\overline{\langle\psi(t)|H^2|\psi(t)\rangle} = d_S^{-2}\mathrm{Tr}[H^2 P_B]e^{-t} + d_S^{-1}d_B^{-1}\mathrm{Tr}[H^2](1-e^{-t}) \,. \tag{C.13}$$

Lastly, we need to specify P_B in (C.8). To start with a simple choice of initial state which becomes increasingly complicated at later times, we assume at $t=0$, S is only entangled with the subsystem $B_1 \in B$ which is adjacent to S (see Fig. 12 for illustration), with $n_{B_1} = n_S$. Therefore, we take:

$$P_B = \mathbf{1}_{B_1} \otimes (|\phi_0\rangle\langle\phi_0|)_{B_2} \tag{C.14}$$

where $|\phi_0\rangle_{B_2}$ is a random product state on B_2. An illustration of whole setting of toy model is given in Fig.12.

Now, plugging in everything, we plot the dynamics of QFI of this toy model in Fig. 12. This should be compared with Fig. 5 (the $t=0$ point in the former should be identified with $t \sim 2$ in the latter). We observe that our BGUE toy model successfully reproduces the following features of the spin chain result in Fig. 5: (i) $F_S(t) \approx F_{B,\mathrm{ent}}(t)$, and both quantities are saturated to a very small number (in this case, the two are precisely equal to the flat spectrum); and (ii) $F_B(t) \approx F_{B,\mathrm{rot}}(t)$ at late times, and they are growing monotonically before saturation.

D Computational basis classical Fisher information

D.1 Full system

In this appendix, we derive the late-time saturation value of the classical Fisher information for measurements in computational basis on the full system $\{|\alpha\rangle\}_{\alpha=1}^d$. d is the total Hilbert space dimension. Using (2), note that we have

$$f^{\mathrm{comp}}(t) = \sum_{\alpha=1}^d \frac{1}{|\langle\alpha|\psi(t)\rangle|^2}|\langle\alpha|[H,|\psi(t)\rangle\langle\psi(t)|]|\alpha\rangle|^2$$
$$= 2\sum_{\alpha=1}^d \langle\alpha|H|\psi(t)\rangle\langle\psi(t)|H|\alpha\rangle - 2\mathrm{Re}\left(\sum_{\alpha=1}^d \langle\alpha|H|\psi(t)\rangle\langle\alpha|H|\psi(t)\rangle\langle\psi(t)|\alpha\rangle/\overline{\langle\psi(t)|\alpha\rangle}\right)$$
$$= 2\langle\psi_0|H^2|\psi_0\rangle - 2\mathrm{Re}\left(\sum_{\alpha=1}^d \langle\alpha|H|\psi(t)\rangle\langle\alpha|H|\psi(t)\rangle\langle\psi(t)|\alpha\rangle/\overline{\langle\psi(t)|\alpha\rangle}\right) \,. \tag{D.1}$$

where the overline indicates complex conjugation. Like in previous calculations, we approximate the late-time state as a typical Haar random state $|\psi_{\mathrm{Haar}}\rangle$. For the present calculation,

1018 we do not need to use the entanglement structure of this state, and can simply use the fact
1019 that the coefficients $z_\nu \equiv \langle \nu | \psi_{\text{Haar}} \rangle$ can be treated as independent complex Gaussian random
1020 variables with zero mean and variance $1/d$, so that we have (In this appendix, we will use the
1021 notation $\langle ... \rangle$ for the Gaussian averages.)

$$\langle z_\mu \bar{z}_\nu \rangle = \delta_{\mu\nu}/d, \quad \langle z_\mu z_\nu \rangle = 0, \quad \langle \bar{z}_\nu / z_\nu \rangle = 0 \tag{D.2}$$

1022 where the last equality follows from that $\bar{z}_\nu / z_\nu$ is a pure phase, and a complex Gaussian random
1023 variable has a uniformly distributed phase.

1024   Using (D.1), we have the following average of f^{comp} over such states:

$$f^{\text{comp}} = \frac{2}{d} \text{Tr}[H^2] - 2 \text{Re} \left(\sum_{\alpha,\beta,\gamma=1}^{d} H_{\alpha\beta} H_{\alpha\gamma} z_\beta z_\gamma \bar{z}_\alpha / z_\alpha \right). \tag{D.3}$$

1025 We organize the sum in the second term above as follows:

$$\sum_{\alpha,\beta,\gamma=1}^{d} H_{\alpha\beta} H_{\alpha\gamma} z_\beta z_\gamma \bar{z}_\alpha / z_\alpha = \sum_{\alpha,\beta=1}^{d} H_{\alpha\beta} H_{\alpha\alpha} z_\beta \bar{z}_\alpha + \sum_{\alpha,\gamma=1}^{d} H_{\alpha\alpha} H_{\alpha\gamma} z_\gamma \bar{z}_\alpha + \sum_{\beta,\gamma \neq \alpha}^{d} H_{\alpha\beta} H_{\alpha\gamma} z_\beta z_\gamma \bar{z}_\alpha / z_\alpha - \sum_{\alpha=1}^{d} H_{\alpha\alpha}^2 |z_\alpha|^2 \tag{D.4}$$

1026 where we sum over $\gamma = \alpha$, $\beta = \alpha$, and $\beta \neq \alpha \wedge \gamma \neq \alpha$ respectively, and in the last term we
1027 subtract the double-counted $\gamma = \beta = \alpha$ case.

1028   Taking the average, we have

$$\langle z_\beta \bar{z}_\alpha \rangle = \delta_{\beta\alpha}/d, \quad \langle z_\beta z_\gamma \bar{z}_\alpha / z_\alpha \rangle = \langle z_\beta z_\gamma \rangle \langle \bar{z}_\alpha / z_\alpha \rangle = 0 \tag{D.5}$$

1029 where the factorization in the second equality follows from independence of the different z_α.

1030   We hence obtain

$$f^{\text{comp}} = \frac{2}{d} \text{Tr}[H^2] - \frac{2}{d} \sum_{\alpha=1}^{d} H_{\alpha\alpha}^2. \tag{D.6}$$

1031 For a local Hamiltonian, both terms are $\mathcal{O}(n)$, explaining the extensive late-time value of f^{comp}
1032 observed for the spin chain model in Fig. 9.

D.2 Subsystem

1034 Now consider the computational basis CFI for a subsystem, f_A^{comp}. We have

$$f_A^{\text{comp}} = \sum_{\alpha=1}^{d_A} \frac{|\langle \alpha | \text{Tr}_{\bar{A}}[H, |\psi\rangle\langle\psi|] |\alpha\rangle|^2}{\langle \alpha | \text{Tr}_{\bar{A}} |\psi\rangle\langle\psi| |\alpha\rangle}$$

$$= \sum_{\alpha=1}^{d_A} \langle \alpha | \text{Tr}_{\bar{A}} |\psi\rangle\langle\psi| |\alpha\rangle^{-1} \sum_{i,j=1}^{d_{\bar{A}}} 2 \Big[\langle \alpha i | H |\psi\rangle\langle\psi| \alpha i\rangle \langle \alpha j |\psi\rangle\langle\psi| H |\alpha j\rangle - \text{Re}\left(\langle \alpha i | H |\psi\rangle\langle\psi| \alpha i\rangle \langle \alpha j | H |\psi\rangle\langle\psi| \alpha j\rangle \right) \Big] \tag{D.7}$$

1035 where we use α and i respectively (and more generally Greek and English small letters respec-
1036 tively) to denote the computational bases in A and $\bar{A}$, and $|\alpha j\rangle \equiv |\alpha\rangle_A |j\rangle_{\bar{A}}$.

1037   In terms of the matrix elements of H in the computational basis, we have

$$f_A^{\text{comp}} = 2 \sum_{\alpha=1}^{d_A} \langle \alpha | \text{Tr}_{\bar{A}} |\psi\rangle\langle\psi| |\alpha\rangle^{-1} \Bigg(\sum_{\gamma,\omega=1}^{d_A} \sum_{i,j,l,p=1}^{d_{\bar{A}}} H_{\alpha i,\gamma l} H_{\omega p,\alpha j} \langle \gamma l |\psi\rangle \langle \psi | \alpha i\rangle \langle \alpha j |\psi\rangle \langle \psi | \omega p\rangle$$

$$- \sum_{\nu,\theta=1}^{d_A} \sum_{i,j,n,t=1}^{d_{\bar{A}}} \text{Re}\left(H_{\alpha i,\nu n} H_{\alpha j,\theta t} \langle \nu n |\psi\rangle \langle \psi | \alpha i\rangle \langle \theta t |\psi\rangle \langle \psi | \alpha j\rangle \right) \Bigg). \tag{D.8}$$

1038   In this appendix, we will assume in all remaining equations that A is always the subsystem
1039 *larger than half* of the full system. Then recall the following approximation for the late-time
1040 state with a flat spectrum,

$$|\psi\rangle = \frac{1}{\sqrt{d_{\bar{A}}}} \sum_{a=1}^{d_{\bar{A}}} |\xi^a\rangle_A |\phi^a\rangle_{\bar{A}} \, , \tag{D.9}$$

1041   where $\{|\xi^a\rangle\}_{a=1}^{d_{\bar{A}}}$ and $\{|\phi^a\rangle\}_{a=1}^{d_{\bar{A}}}$ are independent Haar random pure states of dimension d_A and
1042 $d_{\bar{A}}$ respectively. It follows that

$$\langle \alpha i|\psi\rangle = \frac{1}{\sqrt{d_{\bar{A}}}} \sum_{a=1}^{d_{\bar{A}}} z_\alpha^a x_i^a \tag{D.10}$$

1043   where $\{z_\alpha^a\}_{\alpha,a}$ and $\{x_i^a\}_{a,i}$ are independent complex Gaussians with zero mean and variance
1044 $1/d_A$ and $1/d_{\bar{A}}$ respectively. Using (D.9), we have that the denominator $\langle \alpha|\text{Tr}_{\bar{A}}|\psi\rangle\langle\psi||\alpha\rangle$ is
1045 equal to

$$\langle \alpha|\text{Tr}_{\bar{A}}|\psi\rangle\langle\psi||\alpha\rangle = \frac{1}{d_{\bar{A}}} \sum_{a=1}^{d_{\bar{A}}} \langle \alpha \mid \xi^a\rangle \langle \xi^a \mid \alpha\rangle = \frac{1}{d_{\bar{A}}} \sum_{a=1}^{d_{\bar{A}}} z_\alpha^a \bar{z}_\alpha^a =: s_\alpha \, , \tag{D.11}$$

1046   and s_α has mean $1/d_A$.

1047

1048   In this appendix, we will again use overlines to indicate complex conjugation, and $\langle...\rangle$ to
1049 indicate Gaussian averages. The computational-basis CFI reads,

$$f_A^{\text{comp}} = \frac{2}{d_{\bar{A}}^2} \sum_{\alpha,\gamma,\omega=1}^{d_A} \sum_{i,j,l,p=1}^{d_{\bar{A}}} \sum_{a,b,c,d=1}^{d_{\bar{A}}} H_{\alpha i,\gamma l} H_{\omega p,\alpha j} \, z_\gamma^a x_l^a \bar{z}_\alpha^b \bar{x}_i^b z_\alpha^c x_j^c \bar{z}_\omega^d \bar{x}_p^d / s_\alpha \; (=: I_1)$$

$$- \frac{2}{d_{\bar{A}}^2} \sum_{\alpha,\nu,\theta=1}^{d_A} \sum_{i,j,n,t=1}^{d_{\bar{A}}} \sum_{a,b,c,d=1}^{d_{\bar{A}}} \text{Re}\left(H_{\alpha i,\nu n} H_{\alpha j,\theta t} \, z_\nu^a x_n^a \bar{z}_\alpha^b \bar{x}_i^b z_\theta^c x_t^c \bar{z}_\alpha^d \bar{x}_j^d / s_\alpha\right) \; (=: I_2) \, . \tag{D.12}$$

1050   Now we work on the first term I_1. Taking the average of the Gaussians,

$$\sum_{a,b,c,d=1}^{d_{\bar{A}}} \langle z_\gamma^a x_l^a \bar{z}_\alpha^b \bar{x}_i^b z_\alpha^c x_j^c \bar{z}_\omega^d \bar{x}_p^d / s_\alpha\rangle = \frac{1}{d_{\bar{A}}^2} \sum_{a,c=1}^{d_{\bar{A}}} \langle z_\gamma^a \bar{z}_\alpha^a z_\alpha^c \bar{z}_\omega^c / s_\alpha\rangle \delta_{il}\delta_{jp} + \frac{1}{d_A} \delta_{\gamma\omega}\delta_{lp}\delta_{ij} \, . \tag{D.13}$$

1051   We have

$$I_1 = \frac{2}{d_{\bar{A}}^2} \sum_{\alpha,\gamma,\omega=1}^{d_A} \sum_{i,j,l,p=1}^{d_{\bar{A}}} H_{\alpha i,\gamma l} H_{\omega p,\alpha j} \left(\frac{1}{d_{\bar{A}}^2} \sum_{a,c=1}^{d_{\bar{A}}} \langle z_\gamma^a \bar{z}_\alpha^a z_\alpha^c \bar{z}_\omega^c / s_\alpha\rangle \delta_{il}\delta_{jp} + \frac{1}{d_A} \delta_{\gamma\omega}\delta_{lp}\delta_{ij} \right)$$

$$= \frac{2}{d_{\bar{A}}^4} \sum_{\alpha,\gamma,\omega=1}^{d_A} \sum_{i,j=1}^{d_{\bar{A}}} H_{\alpha i,\gamma i} H_{\omega j,\alpha j} \sum_{a,c=1}^{d_{\bar{A}}} \langle z_\gamma^a \bar{z}_\alpha^a z_\alpha^c \bar{z}_\omega^c / s_\alpha\rangle + \frac{2}{d_{\bar{A}}^2 d_A} \text{Tr}H^2 \, . \tag{D.14}$$

1052   Let's break the first term above into two cases, $\gamma, \omega \neq \alpha$ and $\omega = \gamma = \alpha$, (other cases yield
1053 zero.)

$$\frac{2}{d_{\bar{A}}^4} \sum_{\gamma,\omega\neq\alpha}^{d_A} \sum_{i,j=1}^{d_{\bar{A}}} H_{\alpha i,\gamma i} H_{\omega j,\alpha j} \sum_{a,c=1}^{d_{\bar{A}}} \langle \bar{z}_\alpha^a z_\alpha^c / s_\alpha\rangle \langle z_\gamma^a \bar{z}_\omega^c\rangle + \frac{2}{d_{\bar{A}}^4} \sum_{\alpha=1}^{d_A} \sum_{i,j=1}^{d_{\bar{A}}} H_{\alpha i,\alpha i} H_{\alpha j,\alpha j} \sum_{a,c=1}^{d_{\bar{A}}} \langle z_\alpha^a \bar{z}_\alpha^a z_\alpha^c \bar{z}_\alpha^c / s_\alpha\rangle$$

$$= \frac{2}{d_A d_{\bar{A}}^3} \sum_{\gamma\neq\alpha}^{d_A} \sum_{i,j=1}^{d_{\bar{A}}} H_{\alpha i,\gamma i} H_{\gamma j,\alpha j} + \frac{2}{d_A d_{\bar{A}}^2} \sum_{\alpha=1}^{d_A} \sum_{i,j=1}^{d_{\bar{A}}} H_{\alpha i,\alpha i} H_{\alpha j,\alpha j} = \frac{2}{d_A d_{\bar{A}}^3} \text{Tr}_A H_A^2 + \left(\frac{2}{d_A d_{\bar{A}}^2} - \frac{2}{d_A d_{\bar{A}}^3} \right) \sum_{\alpha=1}^{d_A} (H_A)_{\alpha\alpha}^2 \, .$$

$$\tag{D.15}$$

We hence have

$$
I_1 = \frac{2}{d_A d_{\bar{A}}^2} \mathrm{Tr} H^2 + \frac{2}{d_A d_{\bar{A}}^3} \mathrm{Tr}_A H_A^2 + \left(\frac{2}{d_A d_{\bar{A}}^2} - \frac{2}{d_A d_{\bar{A}}^3} \right) \sum_{\alpha=1}^{d_A} (H_A)_{\alpha\alpha}^2 \,. \tag{D.16}
$$

Now we proceed to I_2. Taking the average of the Gaussians,

$$
\sum_{a,b,c,d=1}^{d_{\bar{A}}} \langle z_\nu^a x_n^a \bar{z}_\alpha^b \bar{x}_i^b z_\theta^c x_t^c \bar{z}_\alpha^d \bar{x}_j^d / s_\alpha \rangle = \frac{1}{d_{\bar{A}}^2} \sum_{a,c=1}^{d_{\bar{A}}} \langle z_\nu^a \bar{z}_\alpha^a z_\theta^c \bar{z}_\alpha^c / s_\alpha \rangle \delta_{ni} \delta_{jt} + \frac{1}{d_{\bar{A}}^2} \sum_{a,b=1}^{d_{\bar{A}}} \langle z_\nu^a \bar{z}_\alpha^b z_\theta^b \bar{z}_\alpha^a / s_\alpha \rangle \delta_{nj} \delta_{it} \tag{D.17}
$$

For I_2 defined in (D.12), we have (we anticipate that the result will be real and drop the "Re"):

$$
I_2 = -\frac{2}{d_{\bar{A}}^4} \sum_{\alpha,\nu,\theta=1}^{d_A} \sum_{i,j,n,t=1}^{d_{\bar{A}}} H_{\alpha i,\nu n} H_{\alpha j,\theta t} \left(\sum_{a,c=1}^{d_{\bar{A}}} \langle z_\nu^a \bar{z}_\alpha^a z_\theta^c \bar{z}_\alpha^c / s_\alpha \rangle \delta_{ni} \delta_{jt} + \sum_{a,b=1}^{d_{\bar{A}}} \langle z_\nu^a \bar{z}_\alpha^b z_\theta^b \bar{z}_\alpha^a / s_\alpha \rangle \delta_{nj} \delta_{it} \right)
$$

$$
= -\frac{2}{d_{\bar{A}}^4} \sum_{\alpha,\nu,\theta=1}^{d_A} \sum_{i,j=1}^{d_{\bar{A}}} H_{\alpha i,\nu i} H_{\alpha j,\theta j} \sum_{a,c=1}^{d_{\bar{A}}} \langle z_\nu^a \bar{z}_\alpha^a z_\theta^c \bar{z}_\alpha^c / s_\alpha \rangle - \frac{2}{d_{\bar{A}}^4} \sum_{\alpha,\nu,\theta=1}^{d_A} \sum_{i,j=1}^{d_{\bar{A}}} H_{\alpha i,\nu j} H_{\alpha j,\theta i} \sum_{a,b=1}^{d_{\bar{A}}} \langle z_\nu^a \bar{z}_\alpha^b z_\theta^b \bar{z}_\alpha^a / s_\alpha \rangle \,. \tag{D.18}
$$

We now break the sums into two cases, $\nu, \theta \neq \alpha$ and $\nu = \theta = \alpha$, (other cases yield zero)

$$
I_2 = -\frac{2}{d_{\bar{A}}^4} \sum_{\nu,\theta \neq \alpha}^{d_A} \sum_{i,j=1}^{d_{\bar{A}}} H_{\alpha i,\nu i} H_{\alpha j,\theta j} \sum_{a,c=1}^{d_{\bar{A}}} \langle z_\nu^a \bar{z}_\alpha^a z_\theta^c \bar{z}_\alpha^c / s_\alpha \rangle - \frac{2}{d_{\bar{A}}^4} \sum_{\alpha}^{d_A} \sum_{i,j=1}^{d_{\bar{A}}} H_{\alpha i,\alpha i} H_{\alpha j,\alpha j} \sum_{a,c=1}^{d_{\bar{A}}} \langle z_\alpha^a \bar{z}_\alpha^a z_\alpha^c \bar{z}_\alpha^c / s_\alpha \rangle
$$

$$
- \frac{2}{d_{\bar{A}}^4} \sum_{\nu,\theta \neq \alpha=1}^{d_A} \sum_{i,j=1}^{d_{\bar{A}}} H_{\alpha i,\nu j} H_{\alpha j,\theta i} \sum_{a,b=1}^{d_{\bar{A}}} \langle z_\nu^a \bar{z}_\alpha^b z_\theta^b \bar{z}_\alpha^a / s_\alpha \rangle - \frac{2}{d_{\bar{A}}^4} \sum_{\alpha=1}^{d_A} \sum_{i,j=1}^{d_{\bar{A}}} H_{\alpha i,\alpha j} H_{\alpha j,\alpha i} \sum_{a,b=1}^{d_{\bar{A}}} \langle z_\alpha^a \bar{z}_\alpha^b z_\alpha^b \bar{z}_\alpha^a / s_\alpha \rangle
$$

$$
= -\frac{2}{d_A d_{\bar{A}}^2} \sum_{\alpha=1}^{d_A} \sum_{i,j=1}^{d_{\bar{A}}} \left(H_{\alpha i,\alpha i} H_{\alpha j,\alpha j} + H_{\alpha i,\alpha j} H_{\alpha j,\alpha i} \right) = -\frac{2}{d_A d_{\bar{A}}^2} \sum_{\alpha=1}^{d_A} \left[(H_A)_{\alpha\alpha}^2 + \mathrm{Tr}_{\bar{A}}(\langle \alpha | H | \alpha \rangle)_{\bar{A}}^2 \right] \,. \tag{D.19}
$$

In conclusion,

$$
f_A^{\mathrm{comp}} = \frac{2}{d_A d_{\bar{A}}^2} \mathrm{Tr} H^2 + \frac{2}{d_A d_{\bar{A}}^3} \mathrm{Tr}_A H_A^2 - \frac{2}{d_A d_{\bar{A}}^3} \sum_{\alpha=1}^{d_A} (H_A)_{\alpha\alpha}^2 - \frac{2}{d_A d_{\bar{A}}^2} \sum_{\alpha=1}^{d_A} \mathrm{Tr}_{\bar{A}}(\langle \alpha | H | \alpha \rangle)_{\bar{A}}^2
$$

$$
\approx \mathcal{O}(n/d_{\bar{A}}) + \mathcal{O}(n_A/d_{\bar{A}}) + \mathcal{O}(n_A/d_{\bar{A}}) + \mathcal{O}(n_A/d_{\bar{A}}) \,. \tag{D.20}
$$

Similarly, we can also calculate the CFI for $\bar{A}$:

$$
f_{\bar{A}}^{\mathrm{comp}} = \frac{2}{d_A^2 d_{\bar{A}}} \mathrm{Tr} H^2 + \frac{2}{d_A^3 d_{\bar{A}}^2} \mathrm{Tr}_{\bar{A}} H_{\bar{A}}^2 - \frac{2}{d_A^3 d_{\bar{A}}^2} \sum_{\alpha=1}^{d_{\bar{A}}} (H_{\bar{A}})_{\alpha\alpha}^2 - \frac{2}{d_A^2 d_{\bar{A}}} \sum_{\alpha=1}^{d_{\bar{A}}} \mathrm{Tr}_A(\langle \alpha | H | \alpha \rangle)_A^2
$$

$$
\approx \mathcal{O}(n/d_A) + \mathcal{O}(n_{\bar{A}}/d_A) + \mathcal{O}(n_{\bar{A}}/d_A) + \mathcal{O}(n_{\bar{A}}/d_A) \,. \tag{D.21}
$$

E   Trace distance between classical probability distributions

Consider the task of distinguishing $|\psi\rangle$ (a Haar state on n-qubit Hilbert space $\mathcal{H}$) and the maximally mixed state ρ_{mm} on $\mathcal{H}$. Let A be a subsystem with n_A qubits and $\bar{A}$ be its complement with

$n_{\bar{A}}$ qubits. We denote the Hilbert space dimensions as $d_A \equiv 2^{n_A}, d_{\bar{A}} \equiv 2^{n_{\bar{A}}}, d \equiv d_A d_{\bar{A}}$. Suppose that the experimentalists who need to perform the task can only perform measurements in the computational basis of A. Then, the total variation distance or trace distance (TD) between the classical probability distributions on d_A bit-strings,

$$\mathrm{TD}_\psi(d, d_{\bar{A}}) \equiv \sum_{i_A=0}^{d_A-1} |p_{i_A} - p'_{i_A}| = \sum_{i_A=0}^{d_A-1} \left| \langle i_A | \mathrm{Tr}_{\bar{A}}(|\psi\rangle\langle\psi|) |i_A\rangle - d_A^{-1} \right| \tag{E.1}$$

would be a good information-theoretic measure of the distinguishability of $|\psi\rangle$ and ρ_{mm} under this restriction. We will average this quantity over Haar-random states $|\psi\rangle$, and find $\mathrm{TD}(d, d_{\bar{A}}) \equiv \overline{\mathrm{TD}_\psi(d, d_{\bar{A}})}$ as a function of $d, d_{\bar{A}}$.

We first state the results, leaving the details to the following two subsections. We first consider the case where we have access to measurements on the full system, namely $d_A = d$ and $d_{\bar{A}} = 1$. We find (see Appendix E.1 for the derivation):

$$\mathrm{TD}(d) \equiv \mathrm{TD}(d, 1) = 2(1 - d^{-1})^d, \quad f(+\infty) = 2e^{-1} \approx 0.735759 \tag{E.2}$$

Next, for $d_A < d$, we find (see Appendix E.2 for derivation):

$$\mathrm{TD}(d, d_{\bar{A}}) = 2 \frac{d_{\bar{A}}^{d_{\bar{A}}-1} (d - d_{\bar{A}})^{d-d_{\bar{A}}} \Gamma(d)}{d^d \Gamma(d_{\bar{A}}) \Gamma(d - d_{\bar{A}})}, \quad \mathrm{TD}(+\infty, d_{\bar{A}}) = 2 \frac{d_{\bar{A}}^{d_{\bar{A}}-1}}{\Gamma(d_{\bar{A}})} e^{-d_{\bar{A}}} = 2(2\pi)^{-1/2} d_{\bar{A}}^{-1/2} + O(d_{\bar{A}}^{-3/2}) \tag{E.3}$$

This is tells us that: (1) When the experimentalists have access to the full system, then the trace distance is $\mathcal{O}(1)$ in thermodynamic limit, indicating that a typical Haar random pure state and a maximally mixed state can be distinguished well. This is similar to the conclusion we arrived at by evaluating the CFI of the computational basis for the full system, f^{comp}, in Sec. D. (2) When the experimentalists even slightly lose control of the full system, they cannot distinguish a typical Haar random pure state and the maximally mixed state well, in the sense that the trace distance in thermodynamic limit is of order $\mathcal{O}(2^{-n_{\bar{A}}/2})$, which is exponentially suppressed in the volume of the complementary subsystem to which the experimentalists have no access. This exponential decaying behaviour is again similar to that of the computational basis CFI of a subsystem, f_A^{comp}.

E.1 Full system

Let $|\psi\rangle$ be a Haar-random state in the d-dimensional Hilbert space $\mathcal{H}$, and $\{|i\rangle, i = 0, ..., d-1\}$ be a fixed orthonormal basis. In this section we want to calculate:

$$\mathrm{TD}(d) = \sum_{i=0}^{d-1} \overline{|\langle i |\psi\rangle\langle\psi| i\rangle - d^{-1}|} = d \cdot \overline{|\langle 0 |\psi\rangle\langle\psi| 0\rangle - d^{-1}|} \tag{E.4}$$

Defining a random variable $x = \langle 0 |\psi\rangle\langle\psi| 0\rangle$, we first calculate its moments $\overline{x^n}$. We use the following formula which calculates the moments of the density matrix:

$$\overline{|\psi\rangle\langle\psi|^{\otimes n}} = \frac{\sum_{\pi \in S_n} \pi}{\sum_{\pi \in S_n} \mathrm{Tr}(\pi)} = \frac{\sum_{\pi \in S_n} \pi}{\sum_{\pi \in S_n} d^{\ell(\pi)}} \tag{E.5}$$

where π is the permutation operator acting on the n-copy Hilbert space $\mathcal{H}^{\otimes n}$, and $\ell(\pi)$ is the number of minimal cycles in π. More precisely, we can define Cayley distance $d_{Cayley}(\pi, \sigma)$ on the permutation group, then $\ell(\pi) = n - d_{Cayley}(\pi, e)$ where e is the identity permutation.

Using the formula

$$\sum_{\pi \in S_n} d^{\ell(\pi)} = \frac{(d-1+n)!}{(d-1)!} \tag{E.6}$$

we obtain:

$$\overline{x^n} = \langle 0^{\otimes n} | \overline{|\psi\rangle\langle\psi|^{\otimes n}} | 0^{\otimes n} \rangle = \frac{\sum_{\pi \in S_n} \langle 0^{\otimes n} | \pi | 0^{\otimes n} \rangle}{\frac{(d-1+n)!}{(d-1)!}} = \frac{n!}{\frac{(d-1+n)!}{(d-1)!}} = \binom{d+n-1}{n}^{-1} \tag{E.7}$$

where we notice that $\langle 0^{\otimes n} | \pi | 0^{\otimes n} \rangle = 1, \forall \pi \in S_n$. Next, we want to calculate the probability density distribution $\rho(x)$ of x. (Note that x itself is a Born-rule probability, which has now become are random variable over different choices of the random pure states $|\psi\rangle$, and we are calculating the probability distribution of x resulting from that of $|\psi\rangle$.) We use the resolvent method, defining

$$R(\lambda) = \overline{(\lambda - x)^{-1}}, \ \rho(\lambda) = -\pi^{-1}\mathrm{Im}[R(\lambda + i0^+)] \tag{E.8}$$

The resolvent can be calculated using the moments to be

$$R(\lambda) = \lambda^{-1} \sum_{n=0}^{\infty} \lambda^{-n} \overline{x^n} = \lambda^{-1} \sum_{n=0}^{\infty} \lambda^{-n} \binom{d+n-1}{n}^{-1} = \lambda^{-1}\,_2F_1(1, 1, d, \lambda^{-1}) \tag{E.9}$$

where $_2F_1(a, b, c, z)$ is the Hypergeometric function. We find that the resulting probability density is

$$\rho(\lambda) = (d-1)(1-\lambda)^{d-2}, \ \lambda \in [0, 1] \tag{E.10}$$

This can be checked for $d = 2, 3$ using the explicit form of the hypergeometric function: $\lambda^{-1}\,_2F_1(1, 1, 2, \lambda^{-1}) = -\log(1 - \lambda^{-1})$ and $\lambda^{-1}\,_2F_1(1, 1, 3, \lambda^{-1}) = 2 + 2(\lambda - 1)\log(1 - \lambda^{-1})$. More generally, by comparing the functional form (E.10) to the numerical evaluation of the RHS of (E.8) in Mathematica, we found exact agreement. In the large d limit, this becomes the Porter-Thomas distribution:

$$p(\lambda) \approx d e^{-\lambda d} . \tag{E.11}$$

Using this form of $\rho(\lambda)$, we obtain:

$$\begin{aligned}
\mathrm{TD}(d) &= d \int_0^1 d\lambda \cdot \rho(\lambda) |\lambda - d^{-1}| = d \int_0^1 d\lambda \cdot (d-1)(1-\lambda)^{d-2} |\lambda - d^{-1}| \\
&= 2(1 - d^{-1})^d
\end{aligned} \tag{E.12}$$

Taking $d \to \infty$, we find:

$$\mathrm{TD}(\infty) = 2e^{-1} \approx 0.735759 . \tag{E.13}$$

For consistency, in the remaining part of this subsection, we report an independent calculation of (E.10) for $d = 2, 3$ using the Bloch vector method.

Calculation using Bloch vector at $d = 2$. As an independent check, let us consider $d = 2$. The result (E.10) predicts that $\rho(\lambda) = 1, \lambda \in [0, 1]$, which is a constant. This seems unusual, but can be confirmed using Bloch vector. A qubit state is given by:

$$|\psi\rangle = \cos(\theta/2)|0\rangle + e^{i\phi}\sin(\theta/2)|1\rangle \tag{E.14}$$

so in this case, we have $x = \langle 0|\psi\rangle\langle\psi|0\rangle = \cos^2(\theta/2)$. The uniform distribution on the Bloch sphere is $\rho(\theta, \phi) = \frac{1}{4\pi}\sin\theta$. Integrating out ϕ, we obtain $\rho(\theta) = \frac{1}{2}\sin\theta$. Changing variables to x, we have:

$$\rho(x) = \rho(\theta) \bigg/ \left|\frac{dx}{d\theta}\right| = \frac{\frac{1}{2}\sin\theta}{2\cos(\theta/2)\sin(\theta/2)\frac{1}{2}} = 1 \tag{E.15}$$

Calculation using Bloch vector at $d = 3$. For SU(3), the Bloch vector is more complicated, but the calculation is still viable. The Haar measure of SU(3) is given by:

$$\mathrm{d}V \propto \sin(2\beta)\sin(2\theta)\sin^2\theta\sin(2b)\,\mathrm{d}\alpha\,\mathrm{d}\beta\,\mathrm{d}\gamma\,\mathrm{d}a\,\mathrm{d}b\,\mathrm{d}c\,\mathrm{d}\theta\,\mathrm{d}\phi\,, \tag{E.16}$$

where the eight Euler angles are within the range:

$$\alpha,\gamma,a,c \in [0,\pi],\ \beta,b,\theta \in [0,\pi/2],\ \phi \in [0,2\pi]\,. \tag{E.17}$$

The SU(3) unitary parametrized by the Euler angles is given by:

$$U = e^{i\lambda_3\alpha}e^{i\lambda_2\beta}e^{i\lambda_3\gamma}e^{i\lambda_5\theta}e^{i\lambda_3 a}e^{i\lambda_2 b}e^{i\lambda_3 c}e^{i\lambda_8\phi} \tag{E.18}$$

where $\lambda_{1\sim 8}$ are eight (3×3) Gell-Mann matrices for generator of $SU(3)$ in fundamental representation (same convention as in Wikipedia). Acting with U on an arbitrary state, say, $(1,0,0)$, we obtain a Bloch vector:

$$|\psi\rangle = U\begin{pmatrix}1\\0\\0\end{pmatrix} = \begin{pmatrix} e^{i(-a+c+\alpha-\gamma+\phi/\sqrt{3})}(e^{i(2a+2\gamma)}\cos b\cos\beta\cos\theta - \sin b\sin\beta) \\ e^{i(-a+c-\alpha-\gamma+\phi/\sqrt{3})}(-e^{i(2a+2\gamma)}\cos b\sin\beta\cos\theta - \sin b\cos\beta) \\ -e^{i(a+c+\phi/\sqrt{3})}\cos b\sin\theta \end{pmatrix}\,. \tag{E.19}$$

For convenience, we study the third component, namely define $x = \cos^2 b\sin^2\theta$. The marginal distribution on (b,θ) is given by $\rho(b,\theta) = 2\sin(2b)\sin(2\theta)\sin^2\theta$. Then the distribution of x is given by:

$$\rho(x) = \int_0^{\pi/2}\int_0^{\pi/2}\mathrm{d}b\,\mathrm{d}\theta\,\rho(b,\theta)\delta(x - \cos^2 b\sin^2\theta) = 2(1-x)\,. \tag{E.20}$$

E.2 Subsystem

We now consider a subsystem of dimension d_A, and use $\{|i\rangle, i_A = 0,...,d_A - 1\}$ to denote an orthonormal basis. We now want to calculate:

$$\mathrm{TD}(d,d_{\bar{A}}) = \sum_{i_A=0}^{d_A-1}\overline{\left|\langle i_A|\mathrm{Tr}_{\bar{A}}(|\psi\rangle\langle\psi|)|i_A\rangle - d_A^{-1}\right|} = d_A\cdot\overline{\left|\langle 0_A|\mathrm{Tr}_{\bar{A}}(|\psi\rangle\langle\psi|)|0_A\rangle - d_A^{-1}\right|}\,. \tag{E.21}$$

Similar to the previous subsection, we define a random variable $x \equiv \langle 0_A|\mathrm{Tr}_{\bar{A}}(|\psi\rangle\langle\psi|)|0_A\rangle$. We first calculate its moments:

$$\overline{x^n} = \langle 0_A^{\otimes n}|\mathrm{Tr}_{\bar{A}_1,...,\bar{A}_n}\left(\overline{|\psi\rangle\langle\psi|^{\otimes n}}\right)|0_A^{\otimes n}\rangle = \frac{\sum_{\pi\in S_n}\langle 0_A^{\otimes n}|\pi_A|0_A^{\otimes n}\rangle\mathrm{Tr}(\pi_{\bar{A}})}{\sum_{\pi\in S_n}\mathrm{Tr}(\pi_A\pi_{\bar{A}})} = \frac{\sum_{\pi\in S_n}d_{\bar{A}}^{\ell(\pi)}}{\sum_{\pi\in S_n}d^{\ell(\pi)}}\,.$$
$$= \binom{d_{\bar{A}}+n-1}{n}\cdot\binom{d+n-1}{n}^{-1} \tag{E.22}$$

Next, we find the resolvent:

$$R(\lambda) = \overline{(\lambda-x)^{-1}} = \lambda^{-1}\sum_{\lambda=0}^{\infty}\lambda^{-n}\overline{x^n} = \lambda^{-1}{}_2F_1(1,d_{\bar{A}},d,\lambda^{-1}) \tag{E.23}$$

Using $\rho(\lambda) = -\pi^{-1}\mathrm{Im}[R(\lambda+i0^+)]$, we obtain the pdf of x, again by using Mathematica:

$$\rho(\lambda) = \frac{\Gamma(d)}{\Gamma(d-d_{\bar{A}})\Gamma(d_{\bar{A}})}(1-\lambda)^{d-d_{\bar{A}}-1}\lambda^{d_{\bar{A}}-1},\ \lambda \in [0,1] \tag{E.24}$$

1134   As a sanity check, one can show that the averaged probability distribution is uniform:

$$\int_0^1 d\lambda \, \rho(\lambda)\lambda = d_A^{-1} \tag{E.25}$$

1135   Now, we can calculate the trace distance:

$$\text{TD}(d, d_{\bar{A}}) = d_A \int_0^1 d\lambda \, \rho(\lambda)|\lambda - d_A^{-1}| = 2\frac{d_{\bar{A}}^{d_{\bar{A}}-1}(d - d_{\bar{A}})^{d-d_{\bar{A}}}\Gamma(d)}{d^d \Gamma(d_{\bar{A}})\Gamma(d - d_{\bar{A}})} \tag{E.26}$$

1136   Now, in order to study the scaling of $f(d, d_{\bar{A}})$, we first take $d = \infty$, and expand around
1137   large but finite $d_{\bar{A}}$:

$$\text{TD}(\infty, d_{\bar{A}}) = 2\frac{d_{\bar{A}}^{d_{\bar{A}}-1}}{\Gamma(d_{\bar{A}})}e^{-d_{\bar{A}}} = 2(2\pi)^{-1/2}d_{\bar{A}}^{-1/2} + O(d_{\bar{A}}^{-3/2}) \tag{E.27}$$

1138   In the last equality, we used the Stirling formula. We therefore see that the trace distance
1139 $\text{TD}(\infty, d_{\bar{A}}) \sim d_{\bar{A}}^{-1/2} \sim 2^{-n_{\bar{A}}/2}$ exponentially decays with the volume of the $\bar{A}$ subsystem.

1140   F   State distinguishability in time estimation code

1141   In this appendix, we will derive the result for $F_H(\rho_R, \sigma_R) = \text{Tr}\sqrt{\rho_R}\sqrt{\sigma_R}$ discussed in (31).
1142   Recall that $\rho_R = \text{Tr}_B |\psi\rangle\langle\psi|$ and $\sigma_R = \text{Tr}_B |\xi\rangle\langle\xi|$. Instead of tuning the relative sizes of R and
1143 B, we label the bipartition as $A\bar{A}$ such that $A \le \bar{A}$. By calculating the $F_H(\rho_A, \sigma_A)$ and $F_H(\rho_{\bar{A}}, \sigma_{\bar{A}})$
1144   and identifying R as A or $\bar{A}$ respectively depending on whether we are before or after the Page
1145   time, we can obtain (31) for any size of R and B.
1146   To simplify calculations, we again use the following simple flat-spectrum random pure
1147   state,

$$|\psi\rangle = \frac{1}{\sqrt{d_A}}\sum_{i=1}^{d_A}|\phi_i\rangle_A U_{ib}|b\rangle_{\bar{A}} . \tag{F.1}$$

1148   The flat entanglement spectrum gives us that

$$\sqrt{\rho_A} \approx \sqrt{d_A}\rho_A , \quad \sqrt{\rho_{\bar{A}}} \approx \sqrt{d_A}\rho_{\bar{A}} . \tag{F.2}$$

1149   It is tricky to evaluate the operator-square-root for σ_A and $\sigma_{\bar{A}}$. We shall go further by approxi-
1150   mating that the entanglement spectrum of ξ is also approximately flat. This is because a local
1151   Hamiltonian cannot drastically change the maximal non-local entanglement across the cut.

$$\sqrt{\sigma_A} \approx \sqrt{d_A}\sigma_A , \quad \sqrt{\sigma_{\bar{A}}} \approx \sqrt{d_A}\sigma_{\bar{A}} . \tag{F.3}$$

1152   We then have

$$F_H(\rho_A, \sigma_A) \approx d_A\text{Tr}\rho_A\sigma_A = \frac{d_A}{d_A^2\sigma^2}\sum_{i,j,k=1}^{d_A}\sum_{a,b,c=1}^{d_{\bar{A}}}U_{ib}\bar{U}_{jc}\langle\phi_k|_A\langle a|_{\bar{A}}\bar{H}|\phi_i\rangle_A|b\rangle_{\bar{A}}\langle\phi_j|_A\langle c|_{\bar{A}}\bar{H}|\phi_k\rangle_A|a\rangle_{\bar{A}} . \tag{F.4}$$

1153   Using the Weingarten calculus,

$$\mathbb{E}_U U_{ib}\bar{U}_{jc} = \frac{1}{d_{\bar{A}}}\delta_{ij}\delta_{bc} \tag{F.5}$$

1154   yields

$$F_H(\rho_A, \sigma_A) \approx \frac{1}{d_A d_{\bar{A}}\sigma^2}\text{Tr}\bar{H}^2 \approx 1 . \tag{F.6}$$

where

$$\mathrm{Tr}\bar{H}^2 = \mathrm{Tr}(H^2 + \langle H\rangle_\psi^2 \mathbf{1} - 2H\langle H\rangle_\psi) \approx dn - (\mathrm{Tr}H)^2/d = dn, \quad \sigma^2 = \mathrm{Tr}H^2/d - (\mathrm{Tr}H/d)^2 \approx n \, . \tag{F.7}$$

We see that for the smaller subsystem A, the noisy codewords are indistinguishable.

Let us now evaluate $F_H(\rho_{\bar{A}}, \sigma_{\bar{A}})$,

$$F_H(\rho_{\bar{A}}, \sigma_{\bar{A}}) \approx d_A \mathrm{Tr}\, \rho_{\bar{A}}\sigma_{\bar{A}} = \frac{d_A}{d_A^2\sigma^2} \sum_{i,j,k,l=1}^{d_A} \sum_{a,b,c,d=1}^{d_{\bar{A}}} U_{ib}\bar{U}_{jc}U_{kd}\bar{U}_{ka} \langle l|_A \langle a|_{\bar{A}} \bar{H} |\phi_i\rangle_A |b\rangle_{\bar{A}} \langle \phi_j|_A \langle c|_{\bar{A}} \bar{H} |l\rangle_A |d\rangle_{\bar{A}} \, . \tag{F.8}$$

Using the Weingarten calculus,

$$\mathbb{E}_U U_{ib}\bar{U}_{jc}U_{kd}\bar{U}_{ka} = \frac{1}{d_{\bar{A}}^2 - 1}(\delta_{ij}\delta_{bc}\delta_{kk}\delta_{da} + \delta_{ik}\delta_{ba}\delta_{kj}\delta_{dc}) \tag{F.9}$$

yields

$$F_H(\rho_{\bar{A}}, \sigma_{\bar{A}}) \approx \frac{d_A \mathrm{Tr}\bar{H}^2 + \mathrm{Tr}\bar{H}_A^2}{d_A d_{\bar{A}}^2 \sigma^2} \approx \frac{d_A dn + d d_{\bar{A}} n_A}{d d_{\bar{A}} n} \approx \frac{n_A}{n} \tag{F.10}$$

where

$$\mathrm{Tr}\bar{H}_{\bar{A}}^2 = \mathrm{Tr}(H_{\bar{A}}^2 + d_{\bar{A}}^2\langle H\rangle_\psi \mathbf{1}_{\bar{A}} - 2d_{\bar{A}}H_{\bar{A}}\langle H\rangle_\psi) \approx d d_{\bar{A}} n_A \approx \frac{n_A}{n} \, . \tag{F.11}$$

Hence, for the larger subsystem $\bar{A}$, the fidelity scales linearly with the system size being traced out.

References

[1] V. Giovannetti, S. Lloyd and L. Maccone, *Quantum metrology*, Physical Review Letters **96**(1), 010401 (2006).

[2] V. Giovannetti, S. Lloyd and L. Maccone, *Advances in quantum metrology*, Nature Photonics **5**(4), 222 (2011).

[3] R. A. Fisher, *On the mathematical foundations of theoretical statistics*, Philosophical transactions of the Royal Society of London. Series A, containing papers of a mathematical or physical character **222**(594-604), 309 (1922).

[4] S. L. Braunstein and C. M. Caves, *Statistical distance and the geometry of quantum states*, Physical Review Letters **72**(22), 3439 (1994).

[5] M. G. Paris, *Quantum estimation for quantum technology*, International Journal of Quantum Information **7**(supp01), 125 (2009).

[6] A. R. Brown and L. Susskind, *Second law of quantum complexity*, Physical Review D **97**(8), 086015 (2018), doi:10.1103/PhysRevD.97.086015, 1701.01107.

[7] J. S. Cotler, D. K. Mark, H.-Y. Huang, F. Hernández, J. Choi, A. L. Shaw, M. Endres and S. Choi, *Emergent Quantum State Designs from Individual Many-Body Wave Functions*, PRX Quantum **4**(1), 010311 (2023), doi:10.1103/PRXQuantum.4.010311, 2103.03536.

[8] J. Cotler, N. Hunter-Jones and D. Ranard, *Fluctuations of subsystem entropies at late times*, Physical Review A **105**(2), 022416 (2022), doi:10.1103/PhysRevA.105.022416.

[9] S. Aaronson, A. Bouland, B. Fefferman, S. Ghosh, U. Vazirani, C. Zhang and Z. Zhou, *Quantum pseudoentanglement*, arXiv:2211.00747 (2022).

[10] X. Feng and M. Ippoliti, *Dynamics of Pseudoentanglement*, arXiv e-prints arXiv:2403.09619 (2024), doi:10.48550/arXiv.2403.09619, 2403.09619.

[11] D. N. Page, *Average entropy of a subsystem*, Physical Review Letters **71**(9), 1291 (1993), doi:10.1103/PhysRevLett.71.1291, gr-qc/9305007.

[12] P. Hayden and J. Preskill, *Black holes as mirrors: quantum information in random subsystems*, Journal of High Energy Physics **2007**(9), 120 (2007), doi:10.1088/1126-6708/2007/09/120, 0708.4025.

[13] S. W. Hawking, *Particle Creation by Black Holes*, Advanced Series in Astrophysics and Cosmology **8**, 85 (1993), doi:10.1142/9789812384935_0005.

[14] S. W. Hawking, *Breakdown of predictability in gravitational collapse*, Physical Review D **14**(10), 2460 (1976), doi:10.1103/PhysRevD.14.2460.

[15] D. N. Page, *Time dependence of Hawking radiation entropy*, Journal of Cosmology and Astroparticle Physics **2013**(9), 028 (2013), doi:10.1088/1475-7516/2013/09/028, 1301.4995.

[16] G. Penington, *Entanglement wedge reconstruction and the information paradox*, Journal of High Energy Physics **2020**(9), 2 (2020), doi:10.1007/JHEP09(2020)002, 1905.08255.

[17] A. Almheiri, N. Engelhardt, D. Marolf and H. Maxfield, *The entropy of bulk quantum fields and the entanglement wedge of an evaporating black hole*, Journal of High Energy Physics **2019**(12), 63 (2019), doi:10.1007/JHEP12(2019)063, 1905.08762.

[18] G. Penington, S. H. Shenker, D. Stanford and Z. Yang, *Replica wormholes and the black hole interior*, Journal of High Energy Physics **2022**(3), 205 (2022), doi:10.1007/JHEP03(2022)205.

[19] A. Almheiri, T. Hartman, J. Maldacena, E. Shaghoulian and A. Tajdini, *Replica wormholes and the entropy of Hawking radiation*, Journal of High Energy Physics **2020**(5), 13 (2020), doi:10.1007/JHEP05(2020)013, 1911.12333.

[20] D. Harlow and P. Hayden, *Quantum computation vs. firewalls*, Journal of High Energy Physics **2013**, 85 (2013), doi:10.1007/JHEP06(2013)085, 1301.4504.

[21] N. Engelhardt and A. C. Wall, *Coarse graining holographic black holes*, Journal of High Energy Physics **2019**(5), 160 (2019), doi:10.1007/JHEP05(2019)160, 1806.01281.

[22] I. Kim, E. Tang and J. Preskill, *The ghost in the radiation: Robust encodings of the black hole interior*, Journal of High Energy Physics **2020**(6), 1 (2020).

[23] A. R. Brown, H. Gharibyan, G. Penington and L. Susskind, *The Python's Lunch: geometric obstructions to decoding Hawking radiation*, Journal of High Energy Physics **2020**(8), 121 (2020), doi:10.1007/JHEP08(2020)121, 1912.00228.

[24] C. Akers, N. Engelhardt, D. Harlow, G. Penington and S. Vardhan, *The black hole interior from non-isometric codes and complexity*, Journal of High Energy Physics **2024**(6), 155 (2024), doi:10.1007/JHEP06(2024)155, 2207.06536.

[25] N. Engelhardt, Å. Folkestad, A. Levine, E. Verheijden and L. Yang, *Spoofing Entanglement in Holography*, arXiv e-prints arXiv:2407.14589 (2024), doi:10.48550/arXiv.2407.14589, 2407.14589.

[26] P. Hauke, M. Heyl, L. Tagliacozzo and P. Zoller, *Measuring multipartite entanglement through dynamic susceptibilities*, Nature Physics **12**(8), 778 (2016), doi:10.1038/nphys3700, 1509.01739.

[27] S. Pappalardi, A. Russomanno, A. Silva and R. Fazio, *Multipartite entanglement after a quantum quench*, Journal of Statistical Mechanics: Theory and Experiment **5**(5), 053104 (2017), doi:10.1088/1742-5468/aa6809, 1701.05883.

[28] M. Brenes, S. Pappalardi, J. Goold and A. Silva, *Multipartite Entanglement Structure in the Eigenstate Thermalization Hypothesis*, Physical Review Letters**124**(4), 040605 (2020), doi:10.1103/PhysRevLett.124.040605, 1909.02980.

[29] P. Faist, M. P. Woods, V. V. Albert, J. M. Renes, J. Eisert and J. Preskill, *Time-energy uncertainty relation for noisy quantum metrology*, PRX Quantum **4**(4), 040336 (2023).

[30] S. Ito and A. Dechant, *Stochastic Time Evolution, Information Geometry, and the Cramér-Rao Bound*, Physical Review X **10**(2), 021056 (2020), doi:10.1103/PhysRevX.10.021056.

[31] D. K. Mark, F. Surace, A. Elben, A. L. Shaw, J. Choi, G. Refael, M. Endres and S. Choi, *Maximum Entropy Principle in Deep Thermalization and in Hilbert-Space Ergodicity*, Physical Review X **14**(4), 041051 (2024), doi:10.1103/PhysRevX.14.041051, 2403.11970.

[32] R. A. Fisher, *Theory of Statistical Estimation*, Proceedings of the Cambridge Philosophical Society **22**(5), 700 (1925), doi:10.1017/S0305004100009580.

[33] E. Lehmann and G. Casella, *Theory of Point Estimation*, Springer (1998).

[34] J. Choi, A. L. Shaw, I. S. Madjarov, X. Xie, R. Finkelstein, J. P. Covey, J. S. Cotler, D. K. Mark, H.-Y. Huang, A. Kale, H. Pichler, F. G. S. L. Brandão *et al.*, *Preparing random states and benchmarking with many-body quantum chaos*, Nature**613**(7944), 468 (2023), doi:10.1038/s41586-022-05442-1, 2103.03535.

[35] W. W. Ho and S. Choi, *Exact Emergent Quantum State Designs from Quantum Chaotic Dynamics*, Physical Review Letters**128**(6), 060601 (2022), doi:10.1103/PhysRevLett.128.060601, 2109.07491.

[36] P. W. Claeys and A. Lamacraft, *Emergent quantum state designs and biunitarity in dual-unitary circuit dynamics*, Quantum **6**, 738 (2022), doi:10.22331/q-2022-06-15-738, 2202.12306.

[37] W. W. Ho and M. Ippoliti, *Solvable model of deep thermalization with distinct design times*, In *APS March Meeting Abstracts*, vol. 2023 of *APS Meeting Abstracts*, p. W33.010 (2023).

[38] S. Popescu, A. J. Short and A. Winter, *Entanglement and the foundations of statistical mechanics*, Nature Physics **2**(11), 754 (2006), doi:10.1038/nphys444, quant-ph/0511225.

[39] Y. Huang and A. W. Harrow, *Instability of localization in translation-invariant systems*, arXiv e-prints arXiv:1907.13392 (2019), doi:10.48550/arXiv.1907.13392, 1907.13392.

[40] S. Pilatowsky-Cameo and S. Choi, *Quantum thermalization of translation-invariant systems at high temperature*, arXiv e-prints arXiv:2409.07516 (2024), doi:10.48550/arXiv.2409.07516, 2409.07516.

[41] S. Guo, M. Sasieta and B. Swingle, *Complexity is not enough for randomness*, SciPost Physics **17**(6), 151 (2024), doi:10.21468/SciPostPhys.17.6.151, 2405.17546.

[42] H. Tang, *Brownian Gaussian Unitary Ensemble: non-equilibrium dynamics, efficient k-design and application in classical shadow tomography*, arXiv 2406.11320 (2024), 2406.11320.

[43] Y. Atas, E. Bogomolny, O. Giraud and G. Roux, *Distribution of the ratio of consecutive level spacings in random matrix ensembles*, Physical Review Letters **110**(8), 084101 (2013).

[44] C. Jonay, D. A. Huse and A. Nahum, *Coarse-grained dynamics of operator and state entanglement*, arXiv e-prints arXiv:1803.00089 (2018), doi:10.48550/arXiv.1803.00089, 1803.00089.

[45] D. A. Roberts, D. Stanford and L. Susskind, *Localized shocks*, Journal of High Energy Physics **2015**, 51 (2015), doi:10.1007/JHEP03(2015)051, 1409.8180.

[46] H. Kim and D. A. Huse, *Ballistic spreading of entanglement in a diffusive nonintegrable system*, Physical Review Letters **111**(12), 127205 (2013).

[47] M. Žnidarič, *Relaxation times of dissipative many-body quantum systems*, Phys. Rev. E **92**, 042143 (2015), doi:10.1103/PhysRevE.92.042143.

[48] D. Harlow, *Jerusalem lectures on black holes and quantum information*, Reviews of Modern Physics **88**(1), 015002 (2016), doi:10.1103/RevModPhys.88.015002, 1409.1231.

[49] J. Eisert, *Entangling Power and Quantum Circuit Complexity*, Physical Review Letters **127**(2), 020501 (2021), doi:10.1103/PhysRevLett.127.020501, 2104.03332.

[50] Z. Ji, Y.-K. Liu and F. Song, *Pseudorandom quantum states*, In *Advances in Cryptology–CRYPTO 2018: 38th Annual International Cryptology Conference, Santa Barbara, CA, USA, August 19–23, 2018, Proceedings, Part III 38*, pp. 126–152. Springer (2018).

[51] S. Boixo, S. V. Isakov, V. N. Smelyanskiy, R. Babbush, N. Ding, Z. Jiang, M. J. Bremner, J. M. Martinis and H. Neven, *Characterizing quantum supremacy in near-term devices*, Nature Physics **14**(6), 595 (2018).

[52] A. Almheiri and H. W. Lin, *The entanglement wedge of unknown couplings*, Journal of High Energy Physics **2022**(8), 62 (2022), doi:10.1007/JHEP08(2022)062, 2111.06298.

[53] H. Liu and S. Vardhan, *Entanglement entropies of equilibrated pure states in quantum many-body systems and gravity*, arXiv e-prints arXiv:2008.01089 (2020), doi:10.48550/arXiv.2008.01089, 2008.01089.

[54] A. Nahum, S. Vijay and J. Haah, *Operator Spreading in Random Unitary Circuits*, Physical Review X **8**(2), 021014 (2018), doi:10.1103/PhysRevX.8.021014, 1705.08975.

[55] C. W. von Keyserlingk, T. Rakovszky, F. Pollmann and S. L. Sondhi, *Operator Hydrodynamics, OTOCs, and Entanglement Growth in Systems without Conservation Laws*, Physical Review X **8**(2), 021013 (2018), doi:10.1103/PhysRevX.8.021013, 1705.08910.

[56] D. E. Parker, X. Cao, A. Avdoshkin, T. Scaffidi and E. Altman, *A Universal Operator Growth Hypothesis*, Physical Review X **9**(4), 041017 (2019), doi:10.1103/PhysRevX.9.041017, 1812.08657.

[57] C. A. Agón, M. Headrick and B. Swingle, *Subsystem complexity and holography*, Journal of High Energy Physics **2019**(2), 1 (2019).

[58] E. Caceres, S. Chapman, J. D. Couch, J. P. Hernandez, R. C. Myers and S.-M. Ruan, *Complexity of mixed states in qft and holography*, Journal of High Energy Physics **2020**(3), 1 (2020).

[59] A. Saha and S. Gangopadhyay, *Holographic study of entanglement and complexity for mixed states*, Physical Review D **103**(8), 086002 (2021).

[60] D. A. Abanin, E. Altman, I. Bloch and M. Serbyn, *Colloquium: Many-body localization, thermalization, and entanglement*, Reviews of Modern Physics **91**(2), 021001 (2019), doi:10.1103/RevModPhys.91.021001, 1804.11065.

[61] S. Moudgalya, B. A. Bernevig and N. Regnault, *Quantum many-body scars and Hilbert space fragmentation: a review of exact results*, Reports on Progress in Physics **85**(8), 086501 (2022), doi:10.1088/1361-6633/ac73a0, 2109.00548.

[62] S. Ryu and T. Takayanagi, *Holographic derivation of entanglement entropy from the anti–de sitter space/conformal field theory correspondence*, Physical Review Letters **96**(18), 181602 (2006).

[63] A. Lewkowycz and J. Maldacena, *Generalized gravitational entropy*, Journal of High Energy Physics **2013**(8), 90 (2013).

[64] T. Faulkner, A. Lewkowycz and J. Maldacena, *Quantum corrections to holographic entanglement entropy*, Journal of High Energy Physics **2013**(11), 74 (2013).

[65] N. Engelhardt and A. C. Wall, *Quantum extremal surfaces: holographic entanglement entropy beyond the classical regime*, Journal of High Energy Physics **2015**(1), 73 (2015).

[66] D. D. Blanco, H. Casini, L.-Y. Hung and R. C. Myers, *Relative entropy and holography*, Journal of High Energy Physics **2013**(8), 1 (2013).

[67] D. L. Jafferis, A. Lewkowycz, J. Maldacena and S. J. Suh, *Relative entropy equals bulk relative entropy*, Journal of High Energy Physics **2016**(6), 1 (2016).

[68] M. Hayashi, *Two quantum analogues of Fisher information from a large deviation viewpoint of quantum estimation*, Journal of Physics A: Mathematical and General **35**(36), 7689 (2002).

[69] D. Petz and C. Ghinea, *Introduction to quantum Fisher information*, In *Quantum Probability and Related Topics*, pp. 261–281. World Scientific (2011).

[70] M. Miyaji, T. Numasawa, N. Shiba, T. Takayanagi and K. Watanabe, *Gravity dual of quantum information metric*, arXiv:1507.07555 (2015).

[71] N. Lashkari and M. Van Raamsdonk, *Canonical energy is quantum Fisher information*, Journal of High Energy Physics **2016**(4), 1 (2016).

[72] S. Banerjee, J. Erdmenger and D. Sarkar, *Connecting fisher information to bulk entanglement in holography*, Journal of High Energy Physics **2018**(8), 1 (2018).

[73] M. Gerbershagen, J. Hernandez, M. Khramtsov and M. Knysh, *Holographic dual of Bures metric and subregion complexity*, arXiv:2412.08707 (2024).

[74] H. Liu and S. J. Suh, *Entanglement growth during thermalization in holographic systems*, Physical Review D **89**(6), 066012 (2014).

[75] T. Hartman and J. Maldacena, *Time evolution of entanglement entropy from black hole interiors*, Journal of High Energy Physics **2013**(5), 1 (2013).

[76] M. Mezei, *On entanglement spreading from holography*, Journal of High Energy Physics **2017**(5), 64 (2017), doi:10.1007/JHEP05(2017)064, 1612.00082.

[77] C. Akers, A. Bouland, L. Chen, T. Kohler, T. Metger and U. Vazirani, *Holographic pseudoentanglement and the complexity of the AdS/CFT dictionary*, arXiv:2411.04978 (2024).

[78] N. Bansal, W.-K. Mok, K. Bharti, D. E. Koh and T. Haug, *Pseudorandom density matrices*, arXiv:2407.11607 (2024).

[79] H. Levine, A. Keesling, A. Omran, H. Bernien, S. Schwartz, A. S. Zibrov, M. Endres, M. Greiner, V. Vuletić and M. D. Lukin, *High-Fidelity Control and Entanglement of Rydberg-Atom Qubits*, Physical Review Letters **121**(12), 123603 (2018), doi:10.1103/PhysRevLett.121.123603, 1806.04682.